Methane and nitrous oxide concentrations and sea-air fluxes in western Long Island Sound, a seasonally hypoxic urban estuary: Hourly to seasonal variability

Cara C. M. Manning[1,#], Anagha Payyambally[1], Josie L. Mottram[1], and Kelsey Ward[1]

[1]University of Connecticut, Department of Marine Sciences, Groton, CT, 06340, USA
[#]Corresponding author: cara.manning@uconn.edu

Abstract. We report the first water column profiles of dissolved methane (CH_4) and nitrous oxide (N_2O) in western Long Island Sound, an urban estuary in which seasonal hypoxia occurs due to eutrophication and restricted exchange with the ocean. We collected samples at seven stations along an 18 km transect in August 2023, October 2023, and May 2024. CH_4 concentrations and sea-air fluxes were highest in August (mean concentration 101 nmol kg^{-1} and mean sea-air flux 154 μmol m^{-2} d^{-1}) and lowest in May (mean concentration 32 nmol kg^{-1} and mean sea-air flux 62 μmol m^{-2} d^{-1}). Conversely, N_2O concentrations and sea-air fluxes were highest in May (mean concentration 12.0 nmol kg^{-1} and mean sea-air flux 4.8 μmol m^{-2} d^{-1}) and lowest in August (mean concentration 10.1 nmol kg^{-1} and mean sea-air flux 2.5 μmol m^{-2} d^{-1}). Surface concentrations of CH_4 and N_2O and sea-air fluxes were highest at the westernmost station in all three seasons. To investigate short-term variability in CH_4, N_2O, and oxygen (O_2), we collected samples every 4 hours over 28 hours at the middle station of the transect, in all three months. Observed changes in gas distributions were linked to water provenance, driven by tidal currents. Our data suggest that there is a persistent source of surface water to western Long Island Sound with high concentrations of CH_4 and N_2O which drives an along-sound gradient in surface concentrations and sea-air fluxes.

Keywords: methane; nitrous oxide; oxygen; hypoxia; estuary; diel cycle

1 Introduction

Long Island Sound (LIS) is an urban estuary that receives wastewater discharge from the most populous city in the USA, New York City, and undergoes seasonal hypoxia. Hypoxic conditions, which are often defined as dissolved oxygen (O_2) concentrations lower than ~64 μmol L^{-1} (~2 mg L^{-1}), can be harmful or fatal to a range of marine life (Diaz and Rosenberg, 2008; Vaquer-Sunyer and Duarte, 2008). Eutrophication (excess nitrogen inputs from human activities, including point source wastewater discharge and runoff) drives overproduction of photosynthetic organisms at the surface and their decomposition at depth, removing O_2 and causing hypoxia in LIS (Parker and O'Reilly, 1991; Varekamp et al., 2014). Hypoxia in LIS is influenced by ongoing climate change: warming temperatures reduce the solubility of O_2 in water and may also increase respiration rates and stratification, both promoting the occurrence of hypoxia (Irby et al., 2018; Parker and O'Reilly, 1991; Whitney and Vlahos, 2021; Wilson et al., 2008). Projected changes in streamflow and associated nitrogen loading may also influence eutrophication and hypoxia in LIS, with regionally variable impacts (Duvall and Hagy, 2025). Other temperate estuaries also experience similar interacting stressors from nutrient pollution and climate change (Howarth et al., 2011; Irby et al., 2018).

Regionally, hypoxia is most severe in western LIS due to the restricted circulation and proximity to the high population density and associated wastewater inputs from New York City (Lee and Lwiza, 2008; Whitney and Vlahos, 2021). Specifically, there are currently six wastewater treatment plants in the East River (a tidal estuary between the island of Manhattan and Brooklyn/Queens which discharges into western LIS) which collectively discharge wastewater from 4 million of the 8 million residents of New York City (NYCDEP, 2025). Although wastewater treatment plan upgrades over recent decades have reduced the amount of nitrogen (N) pollution entering LIS by ~60% from the year 2000 baseline, the 5-year averaged hypoxic area in western LIS has actually increased since 2017 (Duvall et al., 2024; Whitney and Vlahos, 2021). Additionally, prior observations in the East River have demonstrated elevated nutrient levels in this system (Bowman, 1977; Li et al., 2018; Wallace, 2020).

Biochemical reactions involved in organic matter production and decomposition are associated with the production and/or consumption of greenhouse gases including carbon dioxide (CO_2), CH_4, and N_2O (Bange et al., 2010; Reeburgh, 2007). Although the atmospheric concentrations of CH_4 and N_2O are lower than CO_2, CH_4 and N_2O trap heat more effectively and have higher global warming potentials (27 times higher for CH_4 and 273 times higher for N_2O relative to CO_2 on a per mass basis over a 100-year timescale) (Forster et al., 2023). Estuarine greenhouse gas emissions and the relative role of fluxes of CO_2, CH_4 and N_2O in contributing toward the greenhouse effect are highly variable and dynamic (Cai, 2011; Rosentreter et al., 2021; Zheng et al., 2022). Although measurements of benthic N_2O production and groundwater-associated fluxes in LIS have been reported (Mazur et al., 2021; Young et al., 2016), to our knowledge there are no published water column measurements of N_2O or CH_4 concentrations or sea-air fluxes of these gases in LIS. This knowledge gap is significant because high-productivity coastal and estuarine systems experiencing seasonal hypoxia can generate large emissions of these gases, yet reported emissions are widely variable between systems (Capelle and Tortell, 2016; Harley et al., 2015; Kock et al., 2016; Naqvi et al., 2010; Robinson et al., 1998; Rosentreter et al., 2021; Seitzinger et al., 2000; de Wilde and de Bie, 2000; Zheng et al., 2022).

CH_4 is produced and consumed through anaerobic and aerobic processes (Reeburgh, 2007). It is produced during anaerobic methanogenesis, organic matter respiration processes that use carbon as an electron acceptor and result in the formation of CH_4. Anaerobic methanogenesis has previously been reported in LIS sediments in some of the earliest work on marine sedimentary organic matter diagenesis (Martens and Berner, 1974, 1977). Recent work has demonstrated that CH_4

supersaturation in the near-surface ocean may be linked to processes associated with photosynthesis and metabolism of methylated phosphorus and/or sulfur species (Damm et al., 2015; Fazi et al., 2021; Perez-Coronel and Beman, 2022; Repeta et al., 2016). Another study reported that some methylotrophic methanogens inhabiting coastal sediments are oxygen tolerant, and thus CH_4 production may continue even under oxic conditions (Hall et al., 2025). Currently, the importance of aerobic CH_4 production to the CH_4 balance in eutrophic estuarine systems is not well known. In anaerobic systems, CH_4 is consumed through anaerobic oxidation of methane, in which CH_4 is converted to CO_2, and other electron donors such as sulfate (SO_4^{2-}) or nitrate (NO_3^-) are oxidized. This process occurs in anaerobic sediments, and potentially particles, and regulates the amount of CH_4 available to diffuse into the overlying water column. In oxygenated systems, CH_4 is consumed through aerobic oxidation of methane (methanotrophy), conducted by organisms who use methane as their carbon source for organic matter synthesis (Mau et al., 2013; Ward et al., 1987). Methanotrophy can significantly reduce sea-air fluxes of CH_4 (Mau et al., 2013).

N_2O is generated as a byproduct during ammonium oxidation, the first step of nitrification, a chemoautotrophic process that yields energy from the conversion of ammonium to nitrite (NH_4^+ to NO_2^-) (Ward, 2008). Additionally, N_2O is an intermediate in heterotrophic denitrification, an anaerobic organic matter degradation process (Bange et al., 2010). Depending on environmental conditions, this reaction can either be a net source or sink of N_2O, with suboxic conditions tending to favour net N_2O production (incomplete denitrification) and anoxic conditions favouring N_2O consumption (complete denitrification) (Bange et al., 2010; Kock et al., 2016). Additionally, nitrification and denitrification can be coupled through the process of nitrifier denitrification, where the oxidation of NH_4^+ to NO_2^- is followed by reduction of NO_2^- to nitrogen gas (N_2) through intermediates, including N_2O (Wrage et al., 2001).

Here, we report the first measurements of CH_4 and N_2O concentrations and their sea-air fluxes in Long Island Sound, providing new insights into greenhouse gas dynamics in an urbanized, seasonally hypoxic estuary. Using measurements collected at seven stations in three seasons, we characterize seasonal to hourly variability in these gases and place these results in the context of other estuarine studies.

Methods

Sampling locations, timing, and procedures

We collected samples during cruises on the *R/V Connecticut* (2–3 August 2023, 19–20 October 2023, and 22–23 May 2024). On each cruise, we collected water column profiles at the same seven stations spanning an ~18 km transect. These stations were sampled on day 2 over a ~6-hour period, beginning at approximately 07:00 local time at the westernmost station (EXR1) and proceeding sequentially toward the easternmost station (WLI6). Two of the stations were sampled repeatedly: station MID4 was sampled every four hours over a 28-hr period (eight times in total, beginning at ~08:00 on day 1 and continuing until ~12:00 on day 2, and station EXRX was sampled at ~09:00 on day 1 and day 2. For both EXRX and MID4, the final profile was collected as part of the seven-station transect on day 2.

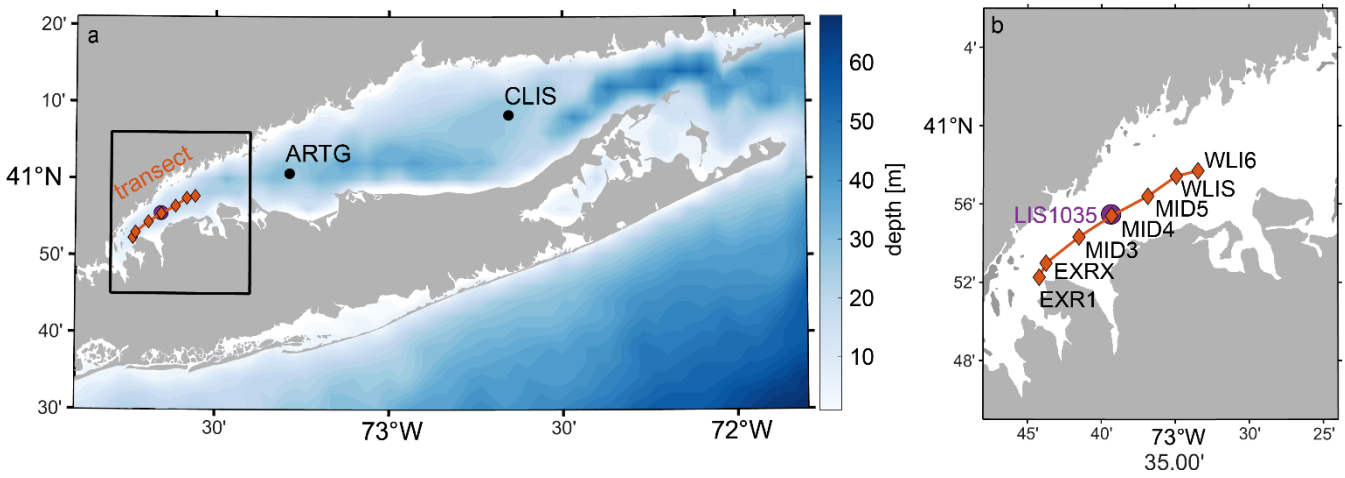

Figure 1. Map of Long Island Sound (a) and the transect sampled (b). The locations of stations sampled on each cruise are shown as orange diamonds and the stations sampled only in May 2024 (ARTG and CLIS) are shown with black circles (a). The station used for current speed predictions (LIS1035) is shown with a purple circle. Maps were generated in MATLAB using m_map (Pawlowicz, 2023).

Additionally, during the May 2024 cruise only, we sampled at stations CLIS and ARTG following the sample collection at WLI6 on day 2. Stations CLIS and ARTG had unique hydrographic properties due to their location closer to the mouth of the inlet. To identify seasonal variability using a consistent dataset, the observations at stations CLIS and ARTG are not included in the discussion and visualizations of this manuscript but are included in the dataset accompanying this manuscript.

Water samples were collected from Niskin bottles attached to a rosette with CTD (Sea-Bird Electronics SBE 9 with SBE 43 dissolved oxygen sensor). Additionally, to get near-bottom water at each station, a Niskin bottle was lowered by hand to ~1 m above the seafloor and manually closed. In total, seven depths were sampled at every station. The shallowest sample on each cast was collected at ~2 m depth and is hereafter referred to as the "surface" sample.

The water sample temperature, salinity, and O_2 data were all taken from the Sea-Bird electronics CTD rosette data. The temperature, salinity, and oxygen data for each near-bottom sample are taken from the CTD data matching with the deepest bottle closed on the corresponding rosette cast. Although a CTD and O_2 sensor attached to a frame without a rosette was deployed by hand to obtain a reading nearer to the bottom, the CTD frame stirred up sediment as it approached the seafloor, leading to erroneous salinity readings and making this method unreliable.

CH_4 and N_2O sample collection and analysis

Water samples for CH_4 and N_2O analysis (duplicates for each depth) were collected into 120 mL glass serum bottles using flexible PVC tubing, with a volume of at least three times the sample volume flowing through the bottle before the sample was sealed. For the August cruise, CH_4/N_2O samples were preserved with 0.5 mL of 8 M potassium hydroxide (KOH) (Magen et al., 2014). For the October and May cruises, CH_4/N_2O samples were preserved with 100 µL of 3.8 g L^{-1} mercuric chloride solution (approximately 50% saturation) (Dickson et al., 2007). Samples were sealed with bromobutyl rubber stoppers and aluminium crimp seals. Analysis was completed within 5 months of each cruise.

Samples were prepared for analysis using headspace equilibration (Magen et al., 2014; de la Paz et al., 2021). Briefly, ~22 mL of water sample was removed while ~22 mL of ultrahigh purity N_2 (5.0 grade) was added. The samples were shaken for approximately 3 hours at room temperature. Then, approximately 20 mL of the headspace was transferred to a 12 mL pre-evacuated vial (Labco Exetainer) by injecting a brine solution (105 mg L^{-1} NaCl) into the bottom of the sample bottle. The Exetainers contained dried KOH to remove CO_2, which can interfere with the quantification of N_2O (Zheng et al., 2008). As part of every sample run, samples of air-equilibrated water at room temperature (~22 ºC) were analysed as a quality assurance measure. Compared to expected results based on atmospheric gas concentrations (2020 ppbv for CH_4 and 338 ppbv for N_2O), the average error for these samples was 0.32 nmol kg^{-1} for CH_4 and 0.07 nmol kg^{-1} for N_2O. The median precision of duplicate field samples was 4 nmol kg^{-1} (7% relative standard deviation) for CH_4 and 0.3 nmol kg^{-1} (3% relative standard deviation) for N_2O.

Samples were calibrated using a standard containing 9.82 ppm CH_4 and 7.97 ppm N_2O in N_2. The certified standard was obtained from Airgas and calibrated internally using an air standard from the NOAA Carbon Cycles and Greenhouse Gas Group (Boulder, Colorado, USA) to reference all data to the WMO scale (Dlugokencky et al., 2020a, b). For each set of samples run, standards of varying concentrations were prepared by mixing the Airgas standard with pure N_2 using Alicat mass flow controllers.

Samples were analysed using an SRI 8610C gas chromatograph with flame ionization detector (FID) for CH_4 and electron capture detector (ECD) for N_2O. An xyzTek Bandolero autosampler was used to transfer the sample into two loops in sequence, with a 2 mL loop going to the FID and 0.25 mL loop going to the ECD. The FID flowpath included a Haysep-D pre-column followed by a Shincarbon column to optimize separation of O_2 and CH_4. For the ECD, there was a Haysep-D pre-column followed by two Haysep-D columns with a vent in between to prevent O_2 from reaching the detector. Backflushing the pre-columns prevented water vapor from entering the main separatory columns. The carrier gas for the FID was N_2 with hydrogen gas (H_2) added to generate the flame, and for the ECD it was N_2 with P5 (95% methane, 5% argon) added as makeup gas.

O_2 sample collection and analysis and correction of in situ O_2 data

To calibrate the SBE 43 oxygen sensor on the rosette, discrete samples for O_2 concentration measurement were collected on several casts on each cruise. Water samples were collected into 140 mL glass biological oxygen demand (BOD) flasks with flared necks using flexible PVC tubing, with at least three times the sample volume flowing through the bottle before the sample was sealed.

O_2 samples were preserved by adding 1 mL of $MnCl_2$ solution and 1 mL of NaI-NaOH solution before inserting a ground glass stopper (Langdon, 2010). The flared neck was filled with water, and the neck and stopper were covered with a latex rubber seal to keep the stopper in place and reduce evaporation. Samples were stored in the dark prior to analysis, which occurred within a few days of each cruise. Analysis was performed via amperometric Winkler titration with a precision of ~0.3% based on the standard deviation of duplicate samples (Langdon, 2010). Due to the slow response time (hysteresis) of the SBE43 O_2 sensor (Bittig et al., 2018; Martini et al., 2007) and strong stratification in the system (the mixed layer depth averaged 5 m) we have visualized and archived the O_2 data using discrete measurements of O_2 from the upcast corresponding to the time when the bottle was closed. On the upcast, the sensor was held at a fixed depth for at least 30 seconds prior to closing each Niskin bottle. On the downcast, the profiler was moving at ~1 m/s and the measured O_2 values lagged behind the in situ values. The discrete O_2 sample data was used to apply a linear correction factor to the O_2 sensor data for each cruise.

Equilibrium concentrations and sea-air flux calculations

In this manuscript, we report the saturation anomaly, Δ, as the concentration or percentage over or undersaturation (depending on context). For O_2:

$$\Delta O_2, \mu\text{mol kg}^{-1} = [O_2]_{\text{meas}} - [O_2]_{\text{eq}} \quad (1)$$

$$\Delta O_2, \% = \frac{[O_2]_{\text{meas}} - [O_2]_{\text{eq}}}{[O_2]_{\text{eq}}} \times 100\% \quad (2)$$

Here $[O_2]_{meas}$ and $[O_2]_{eq}$ are the measured and equilibrium concentrations of O_2, respectively. Equilibrium concentrations were calculated from the measured temperature and salinity following Wiesenburg and Guinasso (1979) for CH_4 and Weiss and Price (1980) for N_2O using MATLAB functions by Manning and Nicholson (2022).

Sea-air gas flux was calculated for CH_4 as follows, and an analogous approach was used for N_2O

$$F = k\left([CH_4]_{\text{meas}} - [CH_4]_{\text{eq}}\right). \quad (3)$$

Here positive values indicate a net sea to air flux (i.e., outgassing), and *k* is the gas transfer velocity calculated with the equation of Wanninkhof et al. (2014), which is a function of the wind speed at 10 m height and the Schmidt number of the gas. Schmidt numbers for CH_4 are calculated based on Jähne et al. (1987) and Schmidt numbers for N_2O are calculated following Wanninkhof (2014), which uses coefficients based on prior publications by Hayduk and Laudie (1974) and Wilke and Chang (1955).

For calculating equilibrium concentrations, the dry atmospheric concentration of CH_4 was assumed to be 2020 ppbv and N_2O was assumed to be 338 ppbv. These concentrations are taken from preliminary surface flask results from Mashpee, Massachusetts, USA (station MSH) from the NOAA Carbon Cycle Greenhouse Gases group website (https://gml.noaa.gov/ccgg/) and represent the average over the three cruises (Dlugokencky et al., 1994, 2020b, a; Hall et al., 2007; Lan et al., 2021). Final surface flask results were not available at the time of submission, but small changes in the atmospheric concentration would have a negligible impact on the calculated sea-air fluxes, relative to other sources of error in the calculations (e.g., the 20% uncertainty in the parameterization of *k* as a function of wind speed). The dry atmospheric concentrations were adjusted to wet concentrations by assuming 100% relative humidity at the air-sea interface and adjusted to local sea level pressure using the mean sea level pressure from the 15 days prior to each measurement which was measured using a mooring at station EXRX, NOAA buoy 44022 (NDBC, 2025). Wind speed was measured on the same mooring and extrapolated from the measurement elevation of 3.5 m to 10 m following Hsu et al. (1994).

Gas transfer velocity is non-linear function of wind speed, i.e., higher wind speeds have a disproportionate effect on the total flux, and therefore gas fluxes calculated based on average wind speeds will underestimate the true flux and fluxes based on instantaneous wind speeds can be biased high or low (Wanninkhof et al., 2009). To account for variability in wind speeds, we determine fluxes using the weighted gas transfer velocity, *k*, calculated following the equation of Teeter et al. (2018), which is modified from Reuer et al. (2007).

$$k = \frac{\sum_{t=1}^{n} f_{open,t}\, k_t\, \omega_t}{\sum_{t=1}^{n} \omega_t} \quad \textbf{(1)}$$

$$\omega_n = 1,\ \omega_{i+1} = (1 - f_{i+1}) \quad (2)$$

$$f_i = \frac{k_i \Delta t}{MLD}, \qquad k_i \Delta t < MLD \quad (3)$$

Here t is the time step, with $t = n$ representing the most recent gas transfer velocity (at the time of sampling), and $t = 1$ the first measurement (15 days prior to the measurement date). The variable f_i is the fraction of the mixed layer ventilated at index i, ω_i is the weighting coefficient at index i, MLD is the mixed layer depth, and Δt is the time interval between each wind speed measurement (15 min).

The mixed layer depth was defined using CTD profiles that were averaged into 1 m depth bins, based on a density difference criterion of 0.125 kg m^{-3} relative to the nearest-surface bin (2–3 m). The mixed layer depth was assumed to be constant in time for the flux calculation. Mixed layer depths ranged from 3–14 m (median 5 m, mean 5.8 m).

Previous publications have discussed what time period should be used when performing weighted flux calculations; a shorter weighting is favored when the residence time of gases in the mixed layer is short (Teeter et al., 2018). Here, a weighting period of 15 days was selected because the mean residence time of both CH_4 and N_2O was 4 days. Additionally, for the October cruise, the meteorological sensors on the buoy at EXRX malfunctioned beginning in September and were replaced 16 days prior to the cruise. For this reason, an integration period longer than 15 days in October was not possible. For May and August, where 30 days of wind speed data was available prior to the cruise, we compared the gas transfer velocities calculated using a weighting period of 15 and 30 days and found that they agreed within 3%.

Typical uncertainty in sea-air gas fluxes was estimated to be 24% for CH_4 and 26% for N_2O using a Monte Carlo error analysis that incorporated the largest known sources of uncertainty (quantified here as relative standard deviation): the parameterization of k as a function of wind speed, at 20% per Wanninkhof et al. (2014); the measured wind speed, at 3% per the manufacturer's specifications; and the gas concentration, at 12% for CH_4 and 4% for N_2O. The uncertainty in the gas concentrations is based on the relative standard deviation of repeat measurements at station MID4 collected over 8 profiles during each cruise; this reflects uncertainty in the fluxes driven by short-term variability in gas concentrations that was not captured by the instantaneous sampling. The uncertainty due to instantaneous sampling is greater than the analytical uncertainty. One potential systematic error that is not captured in our error estimates is lateral variability in wind speed along the transect, which could not be quantified as wind speed data was only available at station EXRX.

Results

Seasonal and spatial trends in hydrography

The sampling months were chosen to reflect the annual variability in O_2 and hydrographic properties in western LIS. We sampled in August 2023 (near the annual maximum extent of hypoxia), October 2023 (following seasonal ventilation of the

subsurface), and May 2024 (near peak river inflow and prior to the onset of hypoxia). The temperature and salinity properties of the water present in western LIS reflect the documented progressive cooling and freshening of the water from August through May (O'Donnell et al., 2008). Specifically, in August, temperature ranged from 20.1 to 24.1 ºC and salinity from 26.0 to 27.0 PSS, in October temperature ranged from 17.0 to 18.1 ºC and salinity from 24.7 to 26.5 PSS, and in May temperature ranged from 11.4 to 17.9 ºC and salinity ranged from 22.4 to 24.2 PSS (Figure 2).

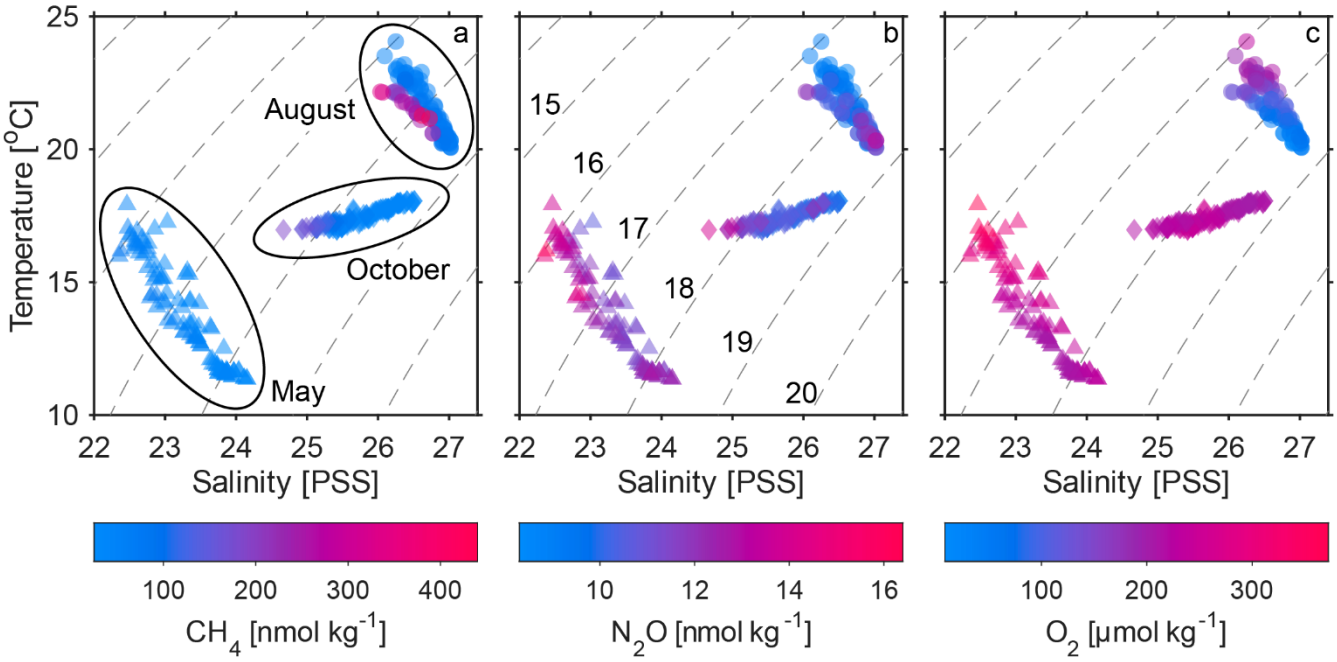

Figure 2. Temperature-salinity plots showing distributions of CH_4 concentration (a), N_2O concentration (b) and O_2 concentration (c) during August (circles), October (diamonds) and May (triangles). In panel a, ellipses indicate the cluster of data points from each month. Dashed lines represent the density anomaly (kg m^{-3}), labelled in panel b. Here all data from all stations is included, including repeat profiles at MID4 and EXRX.

Using transect data at the depths sampled for gases, the in situ temperature, reported as mean (standard deviation) was 21.6 (0.9) ºC in August, 17.4 (0.4) ºC in October, and 13.6 (1.8) ºC in May. Salinity was 26.63 (0.27) PSS in August, 25.71 (0.52) PSS in October, and 23.39 (0.49) PSS in May (Figure 3). Our hydrographic data are consistent with prior observations which showed the annual minimum salinity in LIS typically occurs in May and is associated with peak freshwater inputs from the Connecticut River (~70% the total freshwater discharge to LIS) and other rivers (Lee and Lwiza, 2005; O'Donnell et al., 2014). October displayed the least stratification, and August displayed the strongest stratification and shallowest mixed layer depths. Seasonal cooling due to changes in surface heat flux causes the decline in temperature and stratification over fall and winter (Lee and Lwiza, 2008; O'Donnell et al., 2014). In October, the stratification and thermal gradient reached a minimum, with surface waters typically displaying a lower temperature than the subsurface.

Generally, density and salinity increased from west to east throughout the water column, consistent with prior observations and reflecting the influence of the East River, a tidal strait between Manhattan and Long Island that connects LIS to New York Harbor and the Hudson River (Lee and Lwiza, 2005; O'Donnell et al., 2008). Within the East River, there is two-layer estuarine flow with net surface transport toward LIS and subsurface transport toward New York Harbor, though flow direction can temporarily reverse (Blumberg and Pritchard, 1997; Gay et al., 2004). Surface measurements (~2 m depth) in May displayed

slightly less consistent trends along the transect; although the westernmost station (EXR1) had the lowest salinity and density and the easternmost station (WLI6) had the highest salinity and density, the intermediate stations did not display a consistent east-west gradient. This trend could be driven by local circulation dynamics and/or increased local freshwater sources during our sampling period in May.

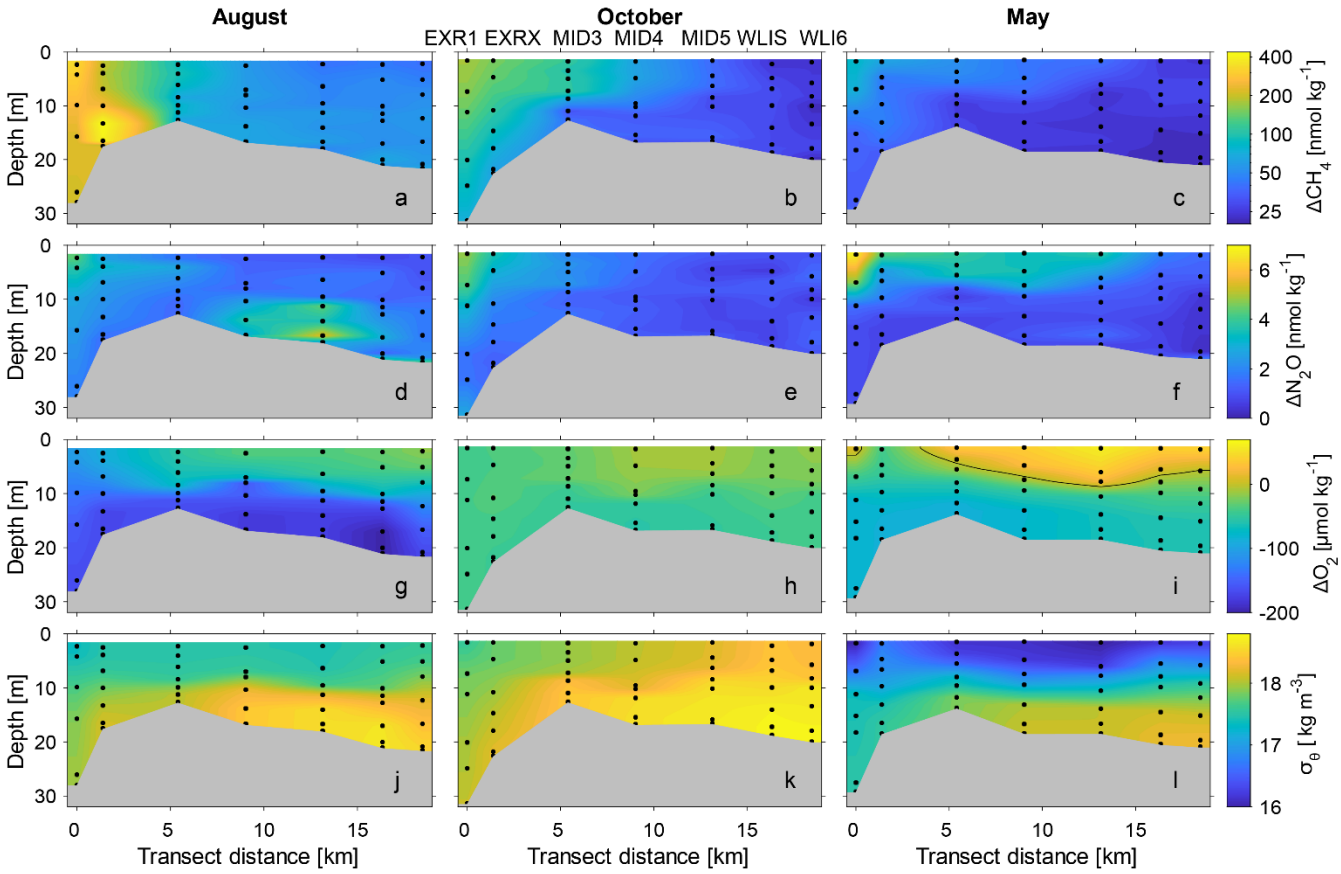

Figure 3. Measurements collected along the 18 km transect in western LIS (depicted in Figure 1). The first three rows show gas saturation anomalies: ΔCH_4 in nmol kg^{-1} (a–c), ΔN_2O in nmol kg^{-1} (d–f), and ΔO_2 in µmol kg^{-1} (g–i). The bottom row is the potential density anomaly in kg m^{-3} (j-l). Note that ΔCH_4 is plotted using a logarithmic scale bar to better display the lateral gradients in each season. The black line on panel i represents equilibrium ($\Delta O_2 = 0$ µmol kg^{-1}); O_2 was undersaturated at all stations along the transect in August and October. The sampling depths are indicated with black circles, and the station names are labelled above panel b.

Seasonal and spatial trends in CH_4, N_2O, and O_2 along the transect in western LIS

Over the three cruises, along the entire transect, CH_4 concentrations ranged from 25–438 nmol kg^{-1} (840–18100 % saturation), N_2O concentrations ranged from 8.4–16.3 nmol kg^{-1} (102–173% saturation), and O_2 concentrations ranged from 8–372 µmol kg^{-1} (4–146% saturation) as reported in Table 1. Evaluating the entire transect, CH_4 concentrations and saturation anomalies were highest in August (mean 119 nmol kg^{-1}, 4900%) and lowest in May (mean 38 nmol kg^{-1}, 1200%). Mean N_2O concentrations were highest in May (mean 12.0 nmol kg^{-1}) and lowest in August (mean 10.1 nmol kg^{-1}), whilst the N_2O saturation anomaly was highest in August (mean 31 %) and lowest in May (mean 18 %). The difference in trends between N_2O concentration and saturation reflects the sensitivity of N_2O solubility to temperature, increasing by ~3–3.5% per °C temperature decrease, and the narrower range in saturation observed for this gas compared to O_2 and CH_4. Water temperature was lowest in

May (mean 13.6 °C) and highest in August (mean 21.6 °C). O_2 concentrations and saturation anomalies were lowest in August (mean 110 µmol kg^{-1}, −52%) and increased to similar levels in October (mean 220 µmol kg^{-1}, −13%) and May (mean 240 µmol kg^{-1}, −13%). However, O_2 was more homogeneous in October (the saturation anomaly had a standard deviation of 5% and O_2 was undersaturated at all depths), compared to May (the saturation anomaly had a standard deviation of 15% and reached a maximum of 24%), consistent with a less stratified water column.

Table 1. Gas distributions, incorporating all measurements along the transect in western LIS from EXR1 to WLI6. Values in square brackets represent the first and third quartile and values in parentheses represent the standard deviation.

	August		October		May	
Parameter	Median	Mean	Median	Mean	Median	Mean
CH_4 concentration (nmol kg^{-1})	68 [58, 194]	119 (101)	43 [32, 98]	67 (44)	32 [29, 45]	38 (13)
CH_4 saturation anomaly (%)	2700 [2300, 8100]	4900 (4200)	1500 [1200, 3600]	2400 (1600)	1000 [900, 1500]	1200 (500)
N_2O concentration (nmol kg^{-1})	9.8 [9.3 10.8]	10.1 (1.1)	10.2 [9.9, 11.0]	10.5 (1.0)	11.6 [11.4, 12.5]	12.0 (1.1)
N_2O saturation anomaly (%)	27 [21, 37]	31 (13)	16 [13, 22]	19 (10)	11 [8, 23]	18 (15)
O_2 concentration (µmol kg^{-1})	89 [69, 159]	110 (52)	217 [210, 231]	220 (14)	231 [211, 260]	240 (34)
O_2 saturation anomaly (%)	−62 [−71, −31]	−52 (23)	−14 [−16, −8]	−13 (5)	−19 [−26, −3]	−13 (15)

The clearest and most seasonally consistent spatial trend along the transects is that the concentrations of CH_4 and N_2O in the upper ~10 m were highest at the westernmost station, EXR1, and generally decreased eastward, and conversely, O_2 generally showed the opposite trend (Figure 3). These trends were observed in all three seasons, despite seasonal changes in the gas concentration ranges. Lateral gradients in O_2 in LIS and more severe O_2 depletion in the far western reaches of LIS is an annual feature of the O_2 dynamics in LIS (O'Donnell et al., 2014; Whitney and Vlahos, 2021). One exception to this trend is in May 2024 where the westernmost station EXR1 had a higher surface O_2 concentration compared to the adjacent station EXRX (276 µmol kg^{-1} at EXR1 compared to 233 µmol kg^{-1} at EXRX). The remaining stations in this transect had higher and similar O_2 concentrations (290 to 323 µmol kg^{-1}). However, the CH_4 and N_2O concentrations at EXRX followed the expected west-east gradient in May (i.e. EXR1 displayed the highest surface concentrations of CH_4 and N_2O). As discussed in the section on hydrography, the surface density anomaly at EXRX was significantly higher than at any other station in the transect (16.8 kg m^{-3} at EXRX compared to 16.0 kg m^{-3} at EXR1 to the west and 16.0 to 16.3 kg m^{-3} at the remaining stations to the east), suggesting the presence of a different mixed layer water mass at EXRX that was not present at the other adjacent stations.

Although O_2 decreased with depth at each station in the transect in all three months (i.e., the bottom water O_2 concentration was always lower than the surface concentration), the vertical gradients in CH_4 and N_2O were more variable. In October and May, five to seven of the seven transect stations had higher CH_4 and N_2O concentrations at the surface compared to the bottom. In August some stations had both surface and subsurface CH_4 and N_2O maxima and the positions of CH_4 and N_2O maxima were notably not coincident. The easternmost stations WLIS and WLI6 consistently displayed the lowest surface CH_4 and N_2O concentrations and the smallest vertical ranges in CH_4 concentration. Comparing CH_4 and N_2O, CH_4 displayed a larger range in concentration and saturation anomaly across the entire transect, as well as a larger range in concentration and saturation anomaly at individual stations on each cruise.

Diel variability in CH_4, N_2O, and O_2 observed in repeat measurements at MID4

We sampled at station MID4 seven times on each cruise, every ~4 hours beginning near 08:00 on day 1. From these data, we aimed to characterize temporal evolution in CH_4, N_2O, and O_2 on sub-daily timescales. Tides in LIS are semidiurnal and display significant spatial variability in timing and magnitude due to the bathymetric constrictions near New York City and the influence of river inflow at multiple points (Bennett et al., 2010; Duvall et al., 2024; McCardell et al., 2016). To identify the direction of water flow at MID4 during each cruise, we used tidal current speed predictions generated by NOAA for 3 and 14 m depth at station LIS1035 (200 m from MID4, Figure 1). NOAA researchers validated the current prediction model for this location through comparison to situ observations which showed a mean error of 8 minutes or less in the timing of flood, slack and ebb, and current speed root mean square error of 0.04 m s^{-1} (NOAA, 2025). The current predictions at both depths indicate that at MID4 during flood tide (positive current speeds), water flows from the northeast, whereas during the ebb tide (negative current speeds), water flows from the southwest.

We found that CH_4 and N_2O concentrations at the surface were influenced by water provenance, frequently showing elevated concentrations in the surface waters during periods when water at MID4 had originated from the southwestern sound, closer to the East River, i.e., during and just following the end of the ebb tide (Figure 4). This result is consistent with transect observations which indicated CH_4 and N_2O concentrations in the upper 10 m were generally highest in western LIS and decreased eastward (Figure 3). The surface CH_4 and N_2O concentrations were lowest in the May samples collected in the second half of the flood tide (11:03 on and 22:57 on day 1) and higher in most profiles obtained near the peak of the ebb tide or just as the tide was switching from ebb to flood (15:03, 19:29, and 03:19).

Additionally, in months where lateral gradients in subsurface gas concentrations occurred, we also observed evidence of tidal influence in the subsurface gas distributions. For example, in August, samples collected at the westernmost stations EXR1 and EXRX had elevated CH_4 concentrations in the samples below 10 m (up to 438 nmol kg^{-1} at EXRX) as compared to the easternmost stations (maximum concentration 68 nmol kg^{-1} at WLI6). Near-bottom CH_4 concentrations at MID4 were elevated in four out of five of the casts collected during ebb tide or just following the end of ebb tide at 14 m depth (day 1 at 08:11 and 19:29, and day 2 at 02:57 and 06:58) and lower in the three casts collected near or following the peak flood (day 1 at 11:03 and 22:57, day 2 at 10:23). Conversely, in August, near-bottom N_2O concentrations did not display a consistent correlation with the tidal cycle, which reflects the lack of a consistent lateral trend in N_2O concentration.

O_2 was also influenced by tidal cycling. From biological processes alone, we would expect mixed layer O_2 to be highest in the late afternoon/early evening due to the accumulation of photosynthetic O_2 during the day, and lowest in the early morning, due to the lack of photosynthesis and continued respiratory consumption overnight (Izett et al., 2024; Nicholson et al., 2015). In August, the sunrise was at approximately 06:10 and the sunset was at 19:42. At MID4, the minimum surface O_2 concentration was reached at 11:03 on day 1 (185 μmol kg^{-1}). The O_2 concentration was significantly higher at 08:11 (210 μmol kg^{-1}), just after the switch from ebb to flood tide. The samples at 08:11 would have been influenced by water originating to the southwest, whereas the samples at 11:03 were collected just after peak flood, and therefore would have been more strongly influenced by the more oxygenated water originating to the northeast. Similarly, the O_2 concentration reached a daily maximum of 231 μmol kg^{-1} in the samples collected at both 15:03 and 19:28. The 19:28 sample was collected just before the end of the ebb tide and therefore would have been influenced by the less oxygenated water to the west, compared to the 15:03 sample which was collected just after the start of ebb tide. Thus, the surface data showed evidence of the expected diel changes in O_2 due to biology, but the cycle was overprinted by tidal influences.

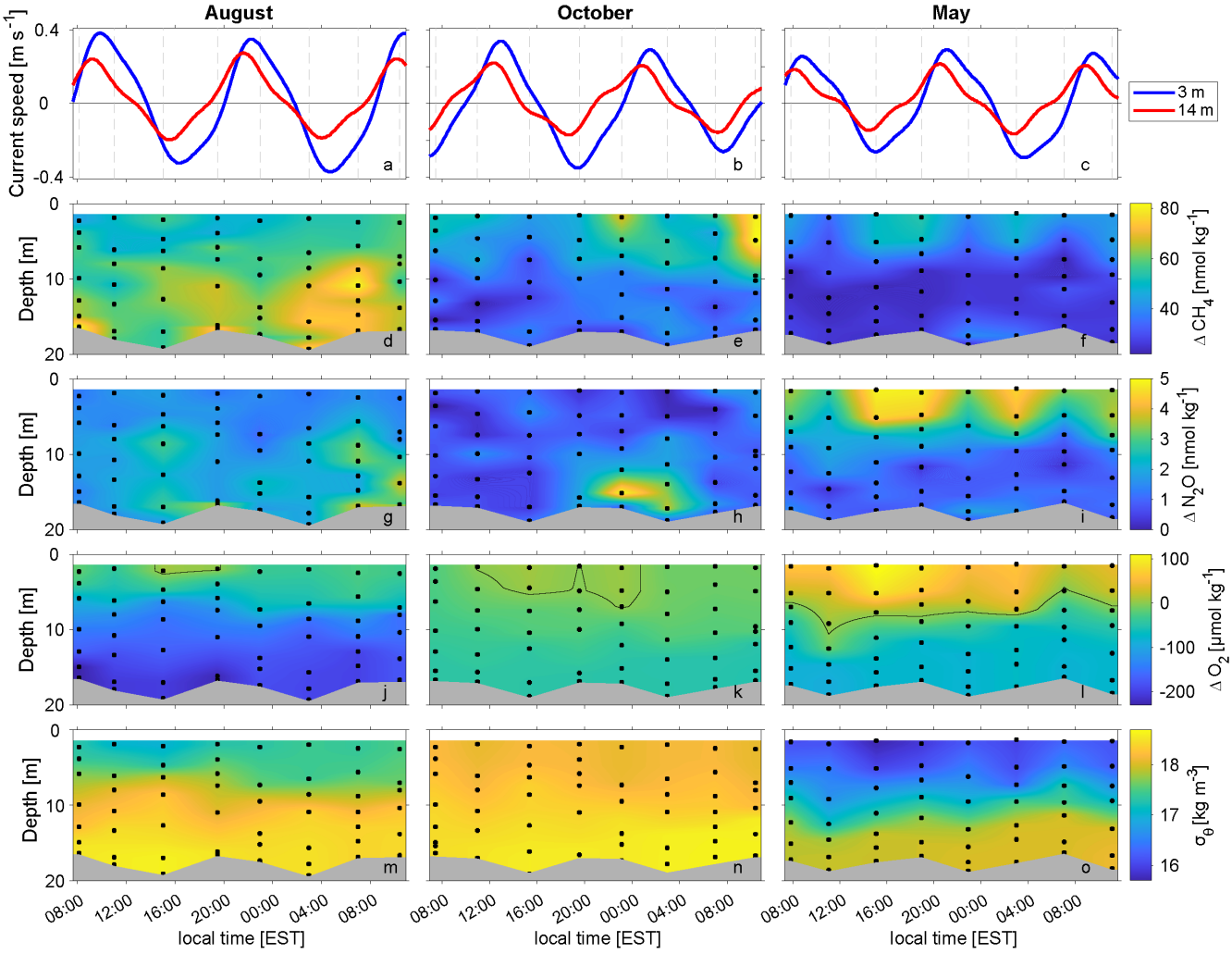

Figure 4. Predicted current speed in m s^{-1} at 3 m and 14 m depth at station LIS1035, near MID4 (a-c). Vertical dashed lines indicate sampling times. Here, positive current speeds indicate flood tide and flow from the northeast. Dissolved gas saturation anomalies collected at station MID4 over a ~28 hr period: ΔCH_4 (d-f), ΔN_2O (g-i), ΔO_2 (j-l), and potential density anomaly (m-o). Black circles indicate sampling times and depths.

Sea-air fluxes of CH_4 and N_2O

We calculated sea-air fluxes of CH_4 and N_2O at each station in each season following the procedures described in the Methods. In all three months, the surface saturation anomalies and sea-air fluxes of both gases were highest at the westernmost station (EXR1) and followed a general decrease toward the east (Figure 5 and Table 2). Using the 15-day weighting method across the seven stations, the mean sea-air CH_4 fluxes (μmol m^{-2} d^{-1}) were 154 in August, 133 in October, and 62 in May, and the mean sea-air N_2O fluxes (μmol m^{-2} d^{-1}) were 2.5 in August, 3.3 in October, and 4.8 in May. Thus, the CH_4 fluxes were highest in August whereas N_2O fluxes were highest in May. The seasonal trends are driven by a combination of seasonal changes in the surface saturation anomaly and the wind speed. Surface saturation anomalies were highest for CH_4 in August (mean 4700%) and highest for N_2O in May (mean 42%), leading to enhanced fluxes in these months, as reported in Table 2. Seasonal variability in wind speed also contributed to seasonal changes in fluxes: the weighted gas transfer velocities were highest in October (k_{CH4} was 1.6 m d^{-1} and k_{N2O} was 1.5 m d^{-1}) and lowest in May (k_{CH4} and k_{N2O} were both 1.2 m d^{-1}) due to the higher wind speeds prior to sampling in October. Thus, the mean N_2O flux was somewhat higher in October compared to August, even though the mean saturation anomaly was slightly higher in August (mean of 25% in August and 23% in October).

To estimate annual mean and median fluxes and surface concentrations, we used the flux and concentration data from August, October, and May and applied a linear interpolation at daily frequency over 1 year. We estimated the annual CH_4 flux to have a mean of 106 µmol m^{-2} d^{-1} and a median of 66 µmol m^{-2} d^{-1} and the annual N_2O flux to have a mean of 3.7 µmol m^{-2} d^{-1} and a median of 3.2 µmol m^{-2} d^{-1}. We estimated the surface CH_4 concentration to have an annual mean of 78 nmol kg^{-1} and a median of 50 nmol kg^{-1}, and the surface N_2O concentration to have an annual mean of 11.5 nmol kg^{-1} and a median of 11.1 nmol kg^{-1}.

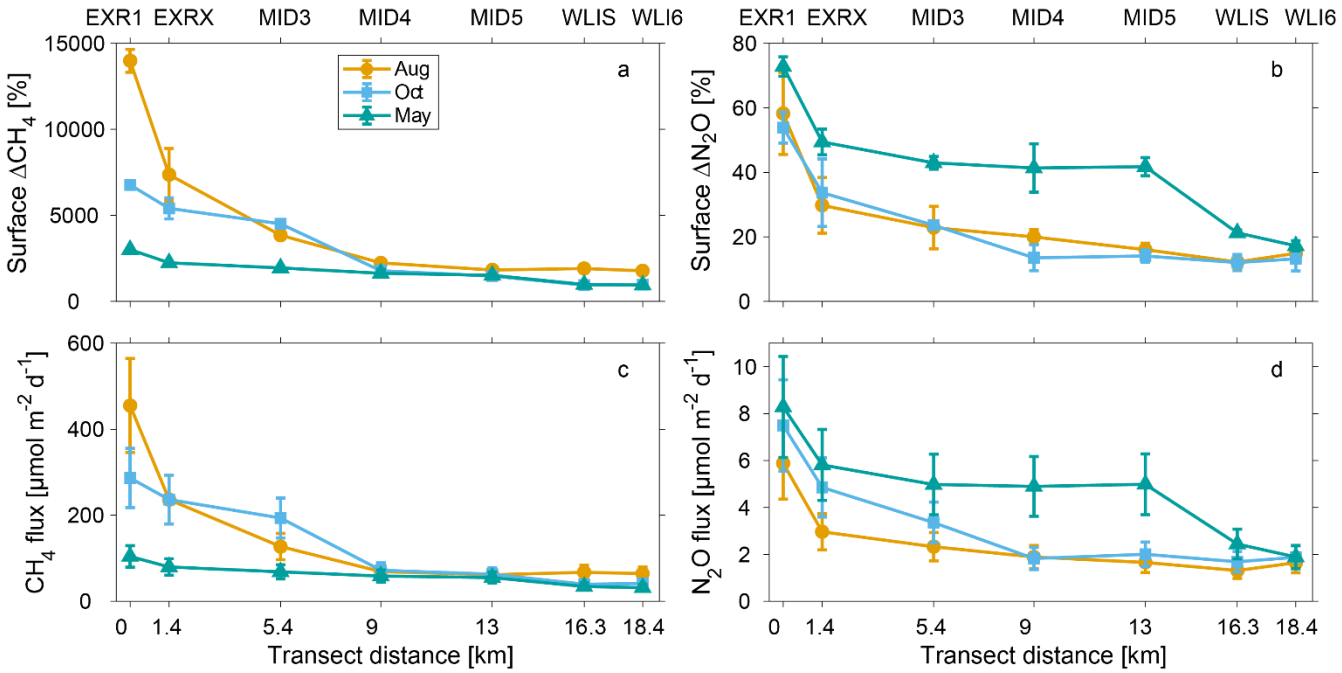

Figure 5. Near-surface saturation anomalies (%) of CH_4 (a) and N_2O (b), in %, and sea-air fluxes (µmol m^{-2} d^{-1}) of CH_4 (c) and N_2O (d) calculated using a 15-day weighting period for each of the seven stations. The transect distance corresponds to the position of each station along the transect, following Figure 1.

Table 2. Sea-air fluxes, surface concentrations, and surface saturation anomalies from all seven stations calculated using 15-day weighting scheme. For medians, values in curly brackets represent the minimum and maximum. For means, values in parentheses represent the standard deviation.

	August		October		May	
Parameter	Median {min, max}	Mean (std.)	Median {min, max}	Mean (std.)	Median {min, max}	Mean (std.)
CH_4 flux (µmol m^{-2} d^{-1})	69 {61, 455}	154 (147)	72 {40, 287}	133 (103)	59 {31, 104}	62 (25)
CH_4 surface concentration (nmol kg^{-1})	54 {44, 335}	114 (109)	50 {28, 185}	86 (64)	48 {28, 86}	51 (21)
CH_4 surface saturation anomaly (%)	2200 {1800, 14000}	4700 (4600)	1800 {900, 6800}	3100 (2400)	1600 {900, 3000}	1800 (700)
N_2O flux (µmol m^{-2} d^{-1})	1.9 {1.3, 5.9}	2.5 (1.6)	2.0 {1.7, 7.5}	3.3 (2.2)	5.0 {1.9, 8.3}	4.8 (2.1)
N_2O surface concentration (nmol kg^{-1})	8.9 {8.4, 12.1}	9.4 (1.3)	10.2 {9.9, 13.9}	11.1 (1.5)	13.1 {10.6, 16.3}	13.1 (1.9)
N_2O surface saturation anomaly (%)	20 {15, 28}	25 (16)	14 {12, 54}	23 (16)	42 {17, 73}	41 (18)

Discussion

We have obtained the first measurements of the greenhouse gases CH_4 and N_2O in western LIS, a eutrophic urban estuary. Although both gases can be generated under processes associated with organic matter remineralization and low-oxygen conditions in subsurface waters, we found that both CH_4 and N_2O often displayed higher concentrations at the surface compared to the subsurface. Both gases showed a lateral (along-estuary) gradient in the near-surface, and surface concentrations were highest at the westernmost station in all three months. The gases displayed different seasonal patterns: the lowest O_2 concentrations and highest CH_4 concentrations were observed in August, the period of maximum hypoxia. The highest N_2O concentrations were observed in May 2024, the month with the coldest water temperatures, partially reflecting the inverse correlation between temperature and solubility for N_2O and indicating that the physical and biogeochemical processes associated with seasonal hypoxia are not the primary driver of N_2O in western LIS. Short-term (sub-daily) variability in CH_4 and N_2O distributions showed a relationship to tides which influence the origin of the water. Below we discuss potential source and sink terms for both gases and reasons for the observed trends. Additionally, we review the sea-air fluxes and surface concentrations in western LIS in the context of recent global compilations for estuarine systems and the global budgets for both gases.

Potential sources and sinks of N_2O to western LIS

The most persistent feature of the N_2O distributions is a concentration maximum in surface waters (upper ~10 m) at the westernmost station which decreased eastward. Additionally, some stations displayed subsurface peaks; in particular, the four easternmost stations in August 2023 all displayed elevated concentrations in near-bottom waters.

N_2O can be produced through both nitrification and denitrification. Water column nitrification rates in oxygenated systems typically increase with reduced competition for NH_4^+ from phytoplankton and decrease with increasing light levels, though different species of ammonia oxidizing archaea and bacteria exhibit different light sensitivities (Proctor et al., 2023; Smith et al., 2014; Ward, 2008). The East River, which flows into western LIS, appears to have conditions primed for nitrification. Total ammonia ($NH_4^+ + NH_3$) concentrations are typically above 5 μmol L^{-1} (and can exceed 40 μmol L^{-1}), NO_2^- is typically above 2 μmol L^{-1} (and can exceed 10 μmol L^{-1}), and NO_3^- is typically above 2 μmol L^{-1} (and can exceed 30 μmol L^{-1}) (Gobler et al., 2006; Li et al., 2018). Comparing conditions in the East River and western LIS, salinity is lower, chlorophyll *a* concentrations are lower, and dissolved inorganic nitrogen (DIN) concentrations are higher in the East River (Bowman, 1977; Li et al., 2018; Wallace and Gobler, 2021), making the East River a net exporter of N to western LIS (Buck et al., 2005; Vlahos et al., 2020). These trends suggest that nitrifiers will experience reduced competition for NH_4^+ in the East River compared to western LIS due to the lower phytoplankton biomass. Euphotic zone depths in the East River are on the order of 4 m (reported range 1–8 m), indicating rapid attenuation of light, which is driven by suspended solids rather than phytoplankton biomass and may cause light limitation of phytoplankton growth in some seasons (Li et al., 2018). Somewhat deeper euphotic zone depths of 5–11 m have been reported for LIS (Anderson and Taylor, 2001; Goebel and Kremer, 2007). Nitrification has previously been reported in the East River from direct incubation measurements in the early 1970s (Chen et al., 1975). The authors found that nitrification rates increased when the salinity of the incubation water was decreased, suggesting nitrifying microbes in the East River are adapted to the fresh water released from the wastewater plants. This result suggests that the East River hosts a unique population of nitrifiers that would not be as active at the higher salinity levels observed in the water in western LIS. Additionally, recent research has proposed that nitrification significantly influences chemical concentrations in the East River (Wallace, 2020; Wallace and Gobler, 2021). Wallace and Gobler (2021) estimated aerobic respiration-driven changes in pH and O_2 by collecting

diurnal profiles from late afternoon to sunrise and found respiration rates to be lower in the East River than in western LIS. They concluded that aerobic respiration could not fully explain the biogeochemical conditions observed in the East River (low total alkalinity, low O_2, low pH, and high pCO_2), and proposed that ammonification of wastewater-derived organic N followed by nitrification could contribute to these observed conditions. It is also possible that denitrification could contribute to the N_2O production in the East River given the high organic N rates and, however, if denitrification in the East River were the primary driver, we would predict to be highest later in the summer following more respiration within the system, rather than in early spring, the start of the productive season.

Overall, the highest N_2O concentration and saturation anomaly in our study was observed in the surface waters at station EXR1 in May, rather than in the stratified subsurface hypoxic waters of August, which we initially hypothesized would have the highest concentrations. Our observations of enhanced N_2O concentrations in the fresh water in the far western LIS suggest that either the N_2O is formed directly in the East River, or the substrates that lead to N_2O production are released from the East River and rapidly converted to N_2O within western LIS. The seasonal increase in surface N_2O saturation anomaly in May corresponds to the annual spring maximum in NH_4^+ concentration (Li et al., 2018) and could relate to decreased utilization of NH_4^+ by phytoplankton over winter and thus increased availability NH_4^+ for nitrifiers. Other studies have reported elevated N_2O concentrations in wastewater effluent and/or downstream of some wastewater treatment plants, though results are highly variable (Burgos et al., 2015; Peterse et al., 2024; Tang et al., 2024b) which may also contribute to the elevated N_2O concentrations observed in the surface waters of western LIS.

We observed transient near-bottom peaks in N_2O at some stations in August and hypothesize that these trends reflect sedimentary sources, either from denitrification or nitrification. These elevated N_2O concentrations did not display a consistent relationship with O_2 (which could suggest a source through water column nitrification). As the water column O_2 concentrations were consistently above the threshold for denitrification to occur (Zakem et al., 2020; Zakem and Follows, 2017), active water column denitrification was not occurring at any of the times and locations we sampled. However, anoxic microenvironments within organisms, aggregates, and suspended/sinking particles may have provided sites for anaerobic metabolic processes to occur (Bianchi et al., 2018; Klawonn et al., 2015; Wan et al., 2023a, b). Mazur et al. (2021) performed sediment core incubations in LIS in summer and winter and found that sediments were on average a small net source of N_2O (mean 8.6 nmol N_2O m^{-2} h^{-1}) but sediment-water fluxes varied widely (range −32 to 68 nmol N_2O m^{-2} h^{-1}). Their incubations also demonstrated evidence of low and spatially variable denitrification rates based on net N_2 fluxes. These observations of spatial variability in sedimentary processes are consistent with our observed variability in the depth-dependent N_2O concentration gradient at adjacent stations with similar bottom-water O_2 concentrations.

In the context of the total N budget in western LIS, N_2O is not a significant source or sink term. Dissolved N_2O concentrations did not exceed 0.016 μmol kg^{-1} in our study, whereas total nitrogen concentrations in western LIS typically exceed 14 μmol kg^{-1} (Vlahos et al., 2020).

Potential sources and sinks of CH_4 in western LIS

Like N_2O, in the upper 10 m, CH_4 generally displayed the highest concentrations at the westernmost station, and concentrations decreased eastward. However, in August, elevated concentrations were observed throughout the water column,

whereas in October and May the highest concentrations generally occurred in the upper water column. As discussed for N_2O, it is likely that the East River strongly influences near-surface CH_4 concentrations in western LIS. Wastewater facilities are known to be significant sources of CH_4; the US EPA greenhouse gas inventory contains a category for CH_4 emissions from treated wastewater effluent (EPA, 2022). This category includes both CH_4 directly released from the wastewater facility and effluent and CH_4 production from the degradation of organic matter downstream of the facility (EPA, 2022). Studies of other wastewater facilities indicate that CH_4 concentrations can peak in wastewater effluent and/or downstream of wastewater plants (Alshboul et al., 2016; Jin et al., 2018; Peterse et al., 2024). Downstream peaks in CH_4 observed in other studies suggest internal production following discharge and may be associated with the high dissolved organic carbon (DOC) concentrations in wastewater effluent. In addition to having high DIN concentrations, the East River contains high DOC concentrations (~200 μmol kg^{-1}) (Buck et al., 2005), which may serve as a substrate for aerobic or anaerobic (sedimentary) methane production, particularly following photodegradation processes following release that increase the bioavailability of DOC (Yin et al., 2021; Yu et al., 2025). Although DOC concentrations are relatively uniform throughout the East River and Long Island Sound (Buck et al., 2005), the wastewater effluent-derived DOC present in the East River will have distinct chemical characteristics compared to the terrestrial-derived DOC and natural marine organic matter present farther east in the estuary and this may affect the yield of CH_4 derived from such DOC.

In general, CH_4 concentrations were higher at the surface than in the subsurface. One notable exception to this trend was the elevated subsurface concentrations at station EXRX sampled during day 2 in August (up to 438 nmol kg^{-1}, higher than the surface). This trend could reflect local sedimentary production occurring driven by organic matter diagenesis and diffusion and/or ebullition transporting CH_4 into the overlying water column (Bange et al., 2010; Valentine, 2011). Given the enhanced subsurface concentrations at EXRX and EXR1 relative to stations to the east, this sedimentary production could be occurring within western LIS or within the East River and be advected into the study area. Sedimentary effluxes of CH_4, particularly in the form of bubbles, can be strongly influenced by pressure, with lower pressure increasing gas efflux (Maeck et al., 2014; Nylund et al., 2025; Römer et al., 2016). Therefore, changes in tidal stage and overlying water depth may drive effluxes of gases and contribute to some of the spatial variability we observe in near-bottom waters for CH_4. Mazur et al. (2021) found using sediment core incubations that LIS sediments at stations EXRX and WLIS had on average net negative CH_4 fluxes in summer, though fluxes were widely variable with some cores showing strongly positive fluxes and others negative fluxes, and such sediment core incubations would not account for tidally-driven effluxes. As for N_2O, it is likely that we are observing effects of transient CH_4 fluxes from the seafloor interacting with the effects of tidal advection causing transient near-bottom peaks in CH_4.

Influence of tides

Our observations at MID4 suggest that tidal flows influence semidiurnal variability in CH_4, N_2O, and O_2 distributions in the upper ~10 m at this station. The influence of tidal cycles on salinity and O_2 in western Long Island Sound has been previously reported. For example, studies using continuous mooring data at station EXRX reported that semidiurnal variability in bottom water O_2 levels are correlated with tidal activity and that tides contribute to both vertical and lateral O_2 transport (Duvall et al., 2024; McCardell et al., 2016). Similar to Duvall et al. (2024), we found that at station MID4, O_2 was influenced by both the diel variability in photosynthesis rates as well as semidiurnal tides. Given the lower frequency of our observations at MID4 (every 4 hr) as compared to previous studies based on mooring observations (every 15 min), we are unable to quantitatively correlate our gas distributions with tides and assess phase lag. Higher frequency measurements of CH_4 and N_2O would be

facilitated by future improvements in sensor technologies to enable accurate in situ measurements of these gases at the observed concentrations. The data presented here provide the first insights demonstrating the influence of tidal dynamics in western LIS on the distributions of CH_4 and N_2O.

Sea-air fluxes and concentrations in the global context

Globally, CH_4 and N_2O concentrations and sea-air fluxes from estuarine systems are highly variable and have a positively skewed distribution. In general, the fluxes we estimate for western LIS are consistent with prior studies which indicated that estuaries play a small role in the global CH_4 and N_2O budgets.

The sea-air CH_4 fluxes we estimate for western LIS (annual mean of 106 μmol m^{-2} d^{-1} and median of 66 μmol m^{-2} d^{-1}) and surface concentrations (annual mean of 78 nmol kg^{-1} and median of 50 nmol kg^{-1}) suggest that CH_4 dynamics in western LIS are consistent with other estuarine systems. A recent global metanalysis by Rosentreter et al. (2021) reported a mean estuarine CH_4 flux of 151 μmol m^{-2} d^{-1} and a median of 38 μmol m^{-2} d^{-1} (N = 53 sites), and a similar study by Zheng et al. (2022) reported a mean diffusive estuarine CH_4 flux of 780 μmol m^{-2} d^{-1} and a median of 120 μmol m^{-2} d^{-1} (N = 91 sites). The estuarine concentrations reported in Zheng et al. (2022) had a mean of 230 nmol kg^{-1} and a median of 110 nmol kg^{-1} – comparable to our results in western LIS. The maximum estuarine concentration reported was 2300 nmol kg^{-1} and the maximum diffusive flux was 27,000 μmol m^{-2} d^{-1} (Zheng et al., 2022). Because of the positively skewed distribution, results for global upscaling of estuarine fluxes are highly sensitive to the dataset and model used (Rosentreter et al., 2021; Zheng et al., 2022). We note that the fluxes we report are for diffusive processes only. Ebullitive fluxes can be a significant contributor to CH_4 emissions in very shallow aquatic systems (bottom depths ~5 m or less), but in deeper systems such as western LIS (bottom depths ranging from 13 to 32 m at the stations in this study), diffusive fluxes will dominate as the vast majority of bubbles released from the sediment will dissolve before reaching the surface (Joyce and Jewell, 2003; West et al., 2016). Globally, estuaries are thought to contribute emissions of 1–6 Tg CH_4 y^{-1} based on mean fluxes from global data compilations (Rosentreter et al., 2021; Zheng et al., 2022), which is ≤1% of global CH_4 emissions from both natural and anthropogenic sources, currently estimated at 540–865 Tg CH_4 y^{-1} (Saunois et al., 2025).

Our N_2O fluxes, estimated to have an annual mean of 3.7 μmol m^{-2} d^{-1} and median of 3.2 μmol m^{-2} d^{-1} are comparable to, though slightly lower than, published typical ranges for estuaries. For example, the global metanalysis of Zheng et al. (2022) reported a median estuarine N_2O water-air flux of 6 μmol m^{-2} d^{-1} and a mean of 19 μmol m^{-2} d^{-1} (maximum 177 μmol m^{-2} d^{-1}) based on 83 studies. Their study demonstrates that a few sites with elevated N_2O significantly influence their global average, causing the mean to be substantially larger than the median. Their median estuarine N_2O concentration of 15 nmol kg^{-1} and mean of 32 nmol kg^{-1} are also comparable, though somewhat higher, than the concentrations we observed (annual mean of 11.5 nmol kg^{-1} and median of 11.1 nmol kg^{-1} for surface waters). Globally, N_2O emissions from inland waters, estuaries and coastal vegetation were recently estimated for 2020 as 0.1 (range 0–0.2) Tg N y^{-1}, which is small in comparison to total net N_2O emissions from all anthropogenic and natural sources, estimated at 18.5 Tg N y^{-1} (range 10.6 to 27.0) from bottom-up approaches (Tian et al., 2024). The study of Zheng et al. (2022) predicted a higher flux from estuaries alone of ~0.25 Tg N y^{-1} indicating that although uncertainty persists in estuarine fluxes due to the uncertainties in upscaling fluxes with a non-normal distribution, estuaries likely play a small role in to the global N_2O budget.

Conclusions

Using the first dataset of dissolved CH_4 and N_2O concentrations in LIS, we find that in spring, summer, and fall, near-surface (upper 10 m) CH_4 and N_2O concentrations were generally highest at the westernmost station (closest to the East River and New York City) and decreased eastward, whereas O_2 showed the opposite trend. Hypoxia is most pronounced in late summer (August), and these low O_2 conditions were associated with elevated CH_4 concentrations and sea-air fluxes. However, N_2O concentrations and fluxes showed more seasonal variability, being highest in May, which may suggest linkages with the annual cycle of primary production. Repeat measurements of CH_4 and N_2O at station MID4 suggested that sub-daily variability in CH_4 and N_2O concentrations were influenced by changes in water provenance (tidal stage). Measurements of O_2 showed some evidence of being associated with photosynthesis.

Our dataset suggests a persistent source of fresh surface water elevated in CH_4 and N_2O (or substrates that support production of these gases) to western LIS which enhances surface concentrations and sea-air fluxes in this region. Given the shallow mixed layer depths in western LIS for most of the year, these concentrations will be quickly released to the atmosphere as the residence time of these gases in the mixed layer is short (4 days on average in our study). We suggest that future work could focus on mapping the distributions of these gases in the East River and in proximity to wastewater inputs. To determine production and consumption mechanisms and rates, water column incubation experiments could be combined with metagenomic analyses (Bourbonnais et al., 2021; Euler et al., 2020; Karl et al., 2008; Rasmussen and Francis, 2022; Uhlig and Loose, 2017). Furthermore, coupled measurements of CO_2, CH_4, and N_2O could contribute to improved accuracy of the relative importance of these three gases in contributing to total greenhouse gas budgets from this region. Western LIS is experiencing ongoing biogeochemical changes including reductions in nutrient loading, warming and associated reductions in O_2 solubility, and acidification driven by increases in atmospheric CO_2 levels (Wallace and Gobler, 2021; Whitney and Vlahos, 2021). Continued monitoring along with targeted experiments evaluating the impacts of multiple stressors would improve predictions of how projected future changes will influence greenhouse gas emissions (Tang et al., 2024a).

Declarations

Ethics approval and consent to participate: Not applicable

Consent for publication: Not applicable

Availability of data and material: The datasets generated during the current study have been prepared for submission to the PANGAEA data repository. We have uploaded the datasets along with the manuscript to the article submission system so that the reviewers and editor can access the data while it awaits publication at PANGAEA.

Competing interests: The authors declare that they have no competing interests.

Funding: Ship time on the *R/V Connecticut* was funded through project R/CMC-20/CTNY funded under award LI-96196201, US Environmental Protection Agency, to the Sponsored Program Services of the University of Connecticut on behalf of Connecticut Sea Grant, and in collaboration with NYSG. The statements, findings, conclusions, views, and recommendations are those of the authors and do not necessarily reflect the views of any of those organizations. Acquisition of data at NOAA mooring 44022 used in this study was supported through the Long Island Sound Integrated Coastal Observatory (LISICOS) which is funded by NOAA. Additional funding for the research was provided by the University of Connecticut.

Authors' contributions: CM, AP, and KW collected samples. CM, AP, JM, and KW analyzed samples. CM analyzed, interpreted, and visualized data and drafted the manuscript. AP, KW, and JM revised the manuscript.

Acknowledgements:
We thank the captain, crew, and science teams on the trips for their support of the research. We thank Julie Granger for providing feedback on a draft of the manuscript.

References

Alshboul, Z., Encinas-Fernández, J., Hofmann, H., and Lorke, A.: Export of Dissolved Methane and Carbon Dioxide with Effluents from Municipal Wastewater Treatment Plants, Environ. Sci. Technol., 50, 5555–5563, https://doi.org/10.1021/acs.est.5b04923, 2016.

Anderson, T. H. and Taylor, G. T.: Nutrient pulses, plankton blooms, and seasonal hypoxia in western Long Island Sound, Estuaries, 24, 228–243, https://doi.org/10.2307/1352947, 2001.

Bange, H. W., Freing, A., Kock, A., and Löscher, C. R.: Marine Pathways to Nitrous Oxide, in: Nitrous Oxide and Climate Change, Routledge, 36–62, 2010.

Bennett, D. C., O'Donnell, J., Bohlen, W. F., and Houk, A.: Tides and Overtides in Long Island Sound, j mar res, 68, 1–35, https://doi.org/10.1357/002224010793079031, 2010.

Bianchi, D., Weber, T. S., Kiko, R., and Deutsch, C.: Global niche of marine anaerobic metabolisms expanded by particle microenvironments, Nature Geosci, 11, 263–268, https://doi.org/10.1038/s41561-018-0081-0, 2018.

Bittig, H. C., Körtzinger, A., Neill, C., van Ooijen, E., Plant, J. N., Hahn, J., Johnson, K. S., Yang, B., and Emerson, S. R.: Oxygen Optode Sensors: Principle, Characterization, Calibration, and Application in the Ocean, Front. Mar. Sci., 4, https://doi.org/10.3389/fmars.2017.00429, 2018.

Blumberg, A. F. and Pritchard, D. W.: Estimates of the transport through the East River, New York, Journal of Geophysical Research: Oceans, 102, 5685–5703, https://doi.org/10.1029/96JC03416, 1997.

Bourbonnais, A., Frey, C., Sun, X., Bristow, L. A., Jayakumar, A., Ostrom, N. E., Casciotti, K. L., and Ward, B. B.: Protocols for Assessing Transformation Rates of Nitrous Oxide in the Water Column, Front. Mar. Sci., 8, https://doi.org/10.3389/fmars.2021.611937, 2021.

Bowman, M. J.: Nutrient distributions and transport in Long Island Sound, Estuarine and Coastal Marine Science, 5, 531–548, https://doi.org/10.1016/0302-3524(77)90100-1, 1977.

Buck, N. J., Gobler, C. J., and Sañudo-Wilhelmy, S. A.: Dissolved Trace Element Concentrations in the East River−Long Island Sound System: Relative Importance of Autochthonous versus Allochthonous Sources, Environ. Sci. Technol., 39, 3528–3537, https://doi.org/10.1021/es048860t, 2005.

Burgos, M., Sierra, A., Ortega, T., and Forja, J. M.: Anthropogenic effects on greenhouse gas (CH4 and N2O) emissions in the Guadalete River Estuary (SW Spain), Science of The Total Environment, 503–504, 179–189, https://doi.org/10.1016/j.scitotenv.2014.06.038, 2015.

Cai, W.-J.: Estuarine and Coastal Ocean Carbon Paradox: CO 2 Sinks or Sites of Terrestrial Carbon Incineration?, Annual Review of Marine Science, 3, 123–145, https://doi.org/10.1146/annurev-marine-120709-142723, 2011.

Capelle, D. W. and Tortell, P. D.: Factors controlling methane and nitrous-oxide variability in the southern British Columbia coastal upwelling system, 179, 56–67, https://doi.org/10.1016/j.marchem.2016.01.011, 2016.

Chen, M., Canelli, E., and Fuhs, G. W.: Effects of Salinity on Nitrification in the East River, Journal (Water Pollution Control Federation), 47, 2474–2481, 1975.

Damm, E., Thoms, S., Beszczynska-Möller, A., Nöthig, E. M., and Kattner, G.: Methane excess production in oxygen-rich polar water and a model of cellular conditions for this paradox, Polar Science, 9, 327–334, https://doi.org/10.1016/j.polar.2015.05.001, 2015.

Diaz, R. J. and Rosenberg, R.: Spreading Dead Zones and Consequences for Marine Ecosystems, Science, 321, 926–929, https://doi.org/10.1126/science.1156401, 2008.

Dlugokencky, E. J., Steele, L. P., Lang, P. M., and Masarie, K. A.: The growth rate and distribution of atmospheric methane, Journal of Geophysical Research: Atmospheres, 99, 17021–17043, https://doi.org/10.1029/94JD01245, 1994.

Dlugokencky, E. J., Crotwell, A. M., Mund, J. W., Crotwell, M. J., and Thoning, K. W.: Atmospheric Methane Dry Air Mole Fractions from the NOAA GML Carbon Cycle Cooperative Global Air Sampling Network, 1983-2019, Version: 2020-07, 2020a.

Dlugokencky, E. J., Crotwell, A. M., Mund, J. W., Crotwell, M. J., and Thoning, K. W.: Atmospheric Nitrous Oxide Dry Air Mole Fractions from the NOAA GML Carbon Cycle Cooperative Global Air Sampling Network, 1997-2019, Version: 2020-07, 2020b.

Duvall, M. S. and Hagy, J. D.: Climate-induced changes in streamflow and nitrogen loading to Long Island Sound, Science of The Total Environment, 992, 179957, https://doi.org/10.1016/j.scitotenv.2025.179957, 2025.

Duvall, M. S., Hagy, J. D., Ammerman, J. W., and Tedesco, M. A.: High-frequency Dissolved Oxygen Dynamics in an Urban Estuary, the Long Island Sound, Estuaries and Coasts, 47, 415–430, https://doi.org/10.1007/s12237-023-01278-8, 2024.

EPA: Inventory of U.S. Greenhouse Gas Emissions and Sinks: 1990-2020. U.S. Environmental Protection Agency, EPA 430-R-22-003, 2022.

Euler, S., Jeffrey, L. C., Maher, D. T., Mackenzie, D., and Tait, D. R.: Shifts in methanogenic archaea communities and methane dynamics along a subtropical estuarine land use gradient, PLOS ONE, 15, e0242339, https://doi.org/10.1371/journal.pone.0242339, 2020.

Fazi, S., Amalfitano, S., Venturi, S., Pacini, N., Vazquez, E., Olaka, L. A., Tassi, F., Crognale, S., Herzsprung, P., Lechtenfeld, O. J., Cabassi, J., Capecchiacci, F., Rossetti, S., Yakimov, M. M., Vaselli, O., Harper, D. M., and Butturini, A.: High concentrations of dissolved biogenic methane associated with cyanobacterial blooms in East African lake surface water, Commun Biol, 4, 845, https://doi.org/10.1038/s42003-021-02365-x, 2021.

Forster, P., Storelvmo, T., and Armour, K.: Chapter 7: The Earth's Energy Budget, Climate Feedbacks, and Climate Sensitivity, in: Climate Change 2021 – The Physical Science Basis: Working Group I Contribution to the Sixth Assessment Report of the Intergovernmental Panel on Climate Change, Cambridge University Press, 923–1054, https://doi.org/10.1017/9781009157896, 2023.

Gay, P. S., O'Donnell, J., and Edwards, C. A.: Exchange between Long Island Sound and adjacent waters, Journal of Geophysical Research: Oceans, 109, https://doi.org/10.1029/2004JC002319, 2004.

Gobler, C. J., Buck, N. J., Sieracki, M. E., and Sañudo-Wilhelmy, S. A.: Nitrogen and silicon limitation of phytoplankton communities across an urban estuary: The East River-Long Island Sound system, Estuarine, Coastal and Shelf Science, 68, 127–138, https://doi.org/10.1016/j.ecss.2006.02.001, 2006.

Goebel, N. and Kremer, J.: Temporal and spatial variability of photosynthetic parameters and community respiration in Long Island Sound, Mar. Ecol. Prog. Ser., 329, 23–42, https://doi.org/10.3354/meps329023, 2007.

Hall, B. D., Dutton, G. S., and Elkins, J. W.: The NOAA nitrous oxide standard scale for atmospheric observations, Journal of Geophysical Research (Atmospheres), 112, 09305, 2007.

Hall, N., Wong, W. W., Lappan, R., Ricci, F., Jeppe, K. J., Glud, R. N., Kawaichi, S., Rotaru, A.-E., Greening, C., and Cook, P. L. M.: Coastal methane emissions driven by aerotolerant methanogens using seaweed and seagrass metabolites, Nat. Geosci., 1–8, https://doi.org/10.1038/s41561-025-01768-3, 2025.

Harley, J. F., Carvalho, L., Dudley, B., Heal, K. V., Rees, R. M., and Skiba, U.: Spatial and seasonal fluxes of the greenhouse gases N2O, CO2 and CH4 in a UK macrotidal estuary, Estuarine, Coastal and Shelf Science, 153, 62–73, https://doi.org/10.1016/j.ecss.2014.12.004, 2015.

Hayduk, W. and Laudie, H.: Prediction of diffusion coefficients for nonelectrolytes in dilute aqueous solutions, AIChE Journal, 20, 611–615, https://doi.org/10.1002/aic.690200329, 1974.

Howarth, R., Chan, F., Conley, D. J., Garnier, J., Doney, S. C., Marino, R., and Billen, G.: Coupled biogeochemical cycles: eutrophication and hypoxia in temperate estuaries and coastal marine ecosystems, Frontiers in Ecology and the Environment, 9, 18–26, https://doi.org/10.1890/100008, 2011.

Hsu, S. A., Meindl, E. A., and Gilhousen, D. B.: Determining the power-law wind-profile exponent under near-neutral stability conditions at sea, Journal of Applied …, 33, 757–765, https://doi.org/10.1175/1520-0450(1994)033%253C0757:DTPLWP%253E2.0.CO;2, 1994.

Irby, I. D., Friedrichs, M. A. M., Da, F., and Hinson, K. E.: The competing impacts of climate change and nutrient reductions on dissolved oxygen in Chesapeake Bay, Biogeosciences, 15, 2649–2668, https://doi.org/10.5194/bg-15-2649-2018, 2018.

Izett, R. W., Fennel, K., Stoer, A. C., and Nicholson, D. P.: Reviews and syntheses: expanding the global coverage of gross primary production and net community production measurements using Biogeochemical-Argo floats, Biogeosciences, 21, 13–47, https://doi.org/10.5194/bg-21-13-2024, 2024.

Jähne, B., Heinz, G., and Dietrich, W.: Measurement of the Diffusion Coefficients of Sparingly Soluble Gases in Water, J Geophys Res, 92, 10767–10776, https://doi.org/10.1029/JC092iC10p10767, 1987.

Jin, H., Yoon, T. K., Begum, M. S., Lee, E.-J., Oh, N.-H., Kang, N., and Park, J.-H.: Longitudinal discontinuities in riverine greenhouse gas dynamics generated by dams and urban wastewater, Biogeosciences, 15, 6349–6369, https://doi.org/10.5194/bg-15-6349-2018, 2018.

Joyce, J. and Jewell, P. W.: Physical controls on methane ebullition from reservoirs and lakes, Environmental & Engineering Geoscience, 9, 167–178, 2003.

Karl, D. M., Beversdorf, L., Björkman, K. M., Church, M. J., Martinez, A., and Delong, E. F.: Aerobic production of methane in the sea, Nature Geosci, 1, 473–478, https://doi.org/10.1038/ngeo234, 2008.

Klawonn, I., Bonaglia, S., Brüchert, V., and Ploug, H.: Aerobic and anaerobic nitrogen transformation processes in N2-fixing cyanobacterial aggregates, ISME J, 9, 1456–1466, https://doi.org/10.1038/ismej.2014.232, 2015.

Kock, A., Arévalo-Martínez, D. L., Löscher, C. R., and Bange, H. W.: Extreme N2O accumulation in the coastal oxygen minimum zone off Peru, Biogeosciences, 13, 827–840, https://doi.org/10.5194/bg-13-827-2016, 2016.

Lan, X., Nisbet, E. G., Dlugokencky, E. J., and Michel, S. E.: What do we know about the global methane budget? Results from four decades of atmospheric CH4 observations and the way forward, Philosophical Transactions of the Royal Society A: Mathematical, Physical and Engineering Sciences, 379, 20200440, https://doi.org/10.1098/rsta.2020.0440, 2021.

Langdon, C.: Determination of dissolved oxygen in seawater by Winkler titration using the amperometric technique, The GO-SHIP Repeat Hydrography Manual: A Collection of Expert Repots and Guidelines, IOCCP Report No. 14, ICPO Publication Series No. 134, 18, 2010.

Lee, Y. J. and Lwiza, K.: Interannual variability of temperature and salinity in shallow water: Long Island Sound, New York, Journal of Geophysical Research: Oceans, 110, https://doi.org/10.1029/2004JC002507, 2005.

Lee, Y. J. and Lwiza, K. M. M.: Characteristics of bottom dissolved oxygen in Long Island Sound, New York, Estuarine, Coastal and Shelf Science, 76, 187–200, https://doi.org/10.1016/j.ecss.2007.07.001, 2008.

Li, Y., Meseck, S. L., Dixon, M. S., and Wikfors, G. H.: The East River tidal strait, New York City, New York, a high-nutrient, low-chlorophyll coastal system, Int Aquat Res, 10, 65–77, https://doi.org/10.1007/s40071-018-0189-2, 2018.

Maeck, A., Hofmann, H., and Lorke, A.: Pumping methane out of aquatic sediments – ebullition forcing mechanisms in an impounded river, Biogeosciences, 11, 2925–2938, https://doi.org/10.5194/bg-11-2925-2014, 2014.

Magen, C., Lapham, L. L., Pohlman, J. W., Marshall, K., Bosman, S., Casso, M., and Chanton, J. P.: A simple headspace equilibration method for measuring dissolved methane, Limnology and Oceanography: Methods, 12, 637–650, https://doi.org/10.4319/lom.2014.12.637, 2014.

Martens, C. S. and Berner, R. A.: Methane Production in the Interstitial Waters of Sulfate-Depleted Marine Sediments, Science, 185, 1167–1169, https://doi.org/10.1126/science.185.4157.1167, 1974.

Martens, C. S. and Berner, R. A.: Interstitial water chemistry of anoxic Long Island Sound sediments. 1. Dissolved gases1, Limnology and Oceanography, 22, 10–25, https://doi.org/10.4319/lo.1977.22.1.0010, 1977.

Martini, M., Butman, B., and Mickelson, M. J.: Long-Term Performance of Aanderaa Optodes and Sea-Bird SBE-43 Dissolved-Oxygen Sensors Bottom Mounted at 32 m in Massachusetts Bay, https://doi.org/10.1175/JTECH2078.1, 2007.

Mau, S., Blees, J., Helmke, E., Niemann, H., and Damm, E.: Vertical distribution of methane oxidation and methanotrophic response to elevated methane concentrations in stratified waters of the Arctic fjord Storfjorden (Svalbard, Norway), Biogeosciences, 10, 6267–6278, https://doi.org/10.5194/bg-10-6267-2013, 2013.

Mazur, C. I., Al-Haj, A. N., Ray, N. E., Sanchez-Viruet, I., and Fulweiler, R. W.: Low denitrification rates and variable benthic nutrient fluxes characterize Long Island Sound sediments, Biogeochemistry, 154, 37–62, https://doi.org/10.1007/s10533-021-00795-7, 2021.

McCardell, G., O'Donnell, J., Souza, A. J., and Palmer, M. R.: Internal tides and tidal cycles of vertical mixing in western Long Island Sound, Journal of Geophysical Research: Oceans, 121, 1063–1084, https://doi.org/10.1002/2015JC010796, 2016.

Naqvi, S. W. A., Bange, H. W., Farías, L., Monteiro, P. M. S., Scranton, M. I., and Zhang, J.: Marine hypoxia/anoxia as a source of CH_4 and N_2O, Biogeosciences, 7, 2159–2190, https://doi.org/10.5194/bg-7-2159-2010, 2010.

Nicholson, D. P., Wilson, S. T., Doney, S. C., and Karl, D. M.: Quantifying subtropical North Pacific gyre mixed layer primary productivity from Seaglider observations of diel oxygen cycles, Geophysical Research Letters, 42, 4032–4039, https://doi.org/10.1002/2015GL063065, 2015.

NOAA: https://tidesandcurrents.noaa.gov/noaacurrents/predictions.html?id=LIS1035_12, last access: 4 October 2025.

NYCDEP: https://www.nyc.gov/site/dep/water/wastewater-treatment-plants.page, last access: 4 October 2025.

Nylund, A. T., Mellqvist, J., Conde, V., Salo, K., Bensow, R., Arneborg, L., Jalkanen, J.-P., Tengberg, A., and Hassellöv, I.-M.: Coastal methane emissions triggered by ship passages, Commun Earth Environ, 6, 380, https://doi.org/10.1038/s43247-025-02344-8, 2025.

O'Donnell, J., Dam, H. G., Bohlen, W. F., Fitzgerald, W., Gay, P. S., Houk, A. E., Cohen, D. C., and Howard-Strobel, M. M.: Intermittent ventilation in the hypoxic zone of western Long Island Sound during the summer of 2004, Journal of Geophysical Research: Oceans, 113, https://doi.org/10.1029/2007JC004716, 2008.

O'Donnell, J., Wilson, R. E., Lwiza, K., Whitney, M., Bohlen, W. F., Codiga, D., Fribance, D. B., Fake, T., Bowman, M., and Varekamp, J.: The Physical Oceanography of Long Island Sound, in: Long Island Sound, edited by: Latimer, J. S., Tedesco, M. A., Swanson, R. L., Yarish, C., Stacey, P. E., and Garza, C., Springer New York, New York, NY, 79–158, https://doi.org/10.1007/978-1-4614-6126-5_3, 2014.

Parker, C. A. and O'Reilly, J. E.: Oxygen Depletion in Long Island Sound: A Historical Perspective, Estuaries, 14, 248–264, 1991.

Pawlowicz, R.: M_Map: A mapping package for MATLAB, 2023.

de la Paz, M., Ferrón, S., Borges, A. V., and Upstill-Goddard, R. C.: Quantification of dissolved methane and nitrous oxide via headspace equilibrium, https://orbi.uliege.be/bitstream/2268/253977/1/SOP5-OCB-Report-v6c.pdf, 2021.

Perez-Coronel, E. and Beman, J. M.: Multiple sources of aerobic methane production in aquatic ecosystems include bacterial photosynthesis, Nat Commun, 13, 6454, https://doi.org/10.1038/s41467-022-34105-y, 2022.

Peterse, I. F., Hendriks, L., Weideveld, S. T. J., Smolders, A. J. P., Lamers, L. P. M., Lücker, S., and Veraart, A. J.: Wastewater-effluent discharge and incomplete denitrification drive riverine CO2, CH4 and N2O emissions, Science of The Total Environment, 951, 175797, https://doi.org/10.1016/j.scitotenv.2024.175797, 2024.

Proctor, C., Coupel, P., Casciotti, K., Tremblay, J.-E., Zakem, E., Arrigo, K. R., and Mills, M. M.: Light, ammonium, pH, and phytoplankton competition as environmental factors controlling nitrification, Limnology and Oceanography, 68, 1490–1503, https://doi.org/10.1002/lno.12359, 2023.

Rasmussen, A. N. and Francis, C. A.: Genome-Resolved Metagenomic Insights into Massive Seasonal Ammonia-Oxidizing Archaea Blooms in San Francisco Bay, mSystems, 7, e01270-21, https://doi.org/10.1128/msystems.01270-21, 2022.

Reeburgh, W.: Oceanic methane biogeochemistry, American Chemical Society, 107, 486–513, https://doi.org/10.1021/cr050362v, 2007.

Repeta, D. J., Ferrón, S., Sosa, O. A., Johnson, C. G., Repeta, L. D., Acker, M., Delong, E. F., and Karl, D. M.: Marine methane paradox explained by bacterial degradation of dissolved organic matter, Nature Geosci, 9, 884–887, https://doi.org/10.1038/ngeo2837, 2016.

Reuer, M., Barnett, B., Bender, M., Falkowski, P., and Hendricks, M.: New estimates of Southern Ocean biological production rates from O2/Ar ratios and the triple isotope composition of O2, Deep Sea Research Part I: Oceanographic Research, 54, 951–974, 2007.

Robinson, A. D., Nedwell, D. B., Harrison, R. M., and Ogilvie, B. G.: Hypernutrified estuaries as sources of N 2 O emission to the atmosphere: the estuary of the River Colne, Essex, UK, Marine Ecology Progress Series, 164, 59–71, 1998.

Römer, M., Riedel, M., Scherwath, M., Heesemann, M., and Spence, G. D.: Tidally controlled gas bubble emissions: A comprehensive study using long-term monitoring data from the NEPTUNE cabled observatory offshore Vancouver Island, Geochem. Geophys. Geosyst., 1–18, https://doi.org/10.1002/2016GC006528, 2016.

Rosentreter, J. A., Borges, A. V., Deemer, B. R., Holgerson, M. A., Liu, S., Song, C., Melack, J., Raymond, P. A., Duarte, C. M., Allen, G. H., Olefeldt, D., Poulter, B., Battin, T. I., and Eyre, B. D.: Half of global methane emissions come from highly variable aquatic ecosystem sources, Nat. Geosci., 14, 225–230, https://doi.org/10.1038/s41561-021-00715-2, 2021.

Saunois, M., Martinez, A., Poulter, B., Zhang, Z., Raymond, P. A., Regnier, P., Canadell, J. G., Jackson, R. B., Patra, P. K., Bousquet, P., Ciais, P., Dlugokencky, E. J., Lan, X., Allen, G. H., Bastviken, D., Beerling, D. J., Belikov, D. A., Blake, D. R., Castaldi, S., Crippa, M., Deemer, B. R., Dennison, F., Etiope, G., Gedney, N., Höglund-Isaksson, L., Holgerson, M. A., Hopcroft, P. O., Hugelius, G., Ito, A., Jain, A. K., Janardanan, R., Johnson, M. S., Kleinen, T., Krummel, P. B., Lauerwald, R., Li, T., Liu, X., McDonald, K. C., Melton, J. R., Mühle, J., Müller, J., Murguia-Flores, F., Niwa, Y., Noce, S., Pan, S., Parker, R. J., Peng, C., Ramonet, M., Riley, W. J., Rocher-Ros, G., Rosentreter, J. A., Sasakawa, M., Segers, A., Smith, S. J., Stanley, E. H., Thanwerdas, J., Tian, H., Tsuruta, A., Tubiello, F. N., Weber, T. S., van der Werf, G. R., Worthy, D. E. J., Xi, Y., Yoshida, Y., Zhang, W., Zheng, B., Zhu, Q., Zhu, Q., and Zhuang, Q.: Global Methane Budget 2000–2020, Earth System Science Data, 17, 1873–1958, https://doi.org/10.5194/essd-17-1873-2025, 2025.

Seitzinger, S. P., Kroeze, C., and Styles, R. V.: Global distribution of N2O emissions from aquatic systems: natural emissions and anthropogenic effects, Chemosphere: Global Change Science, 2, 267–279, https://doi.org/10.1016/S1465-9972(00)00015-5, 2000.

Smith, J. M., Chavez, F. P., and Francis, C. A.: Ammonium Uptake by Phytoplankton Regulates Nitrification in the Sunlit Ocean, PLoS ONE, 9, e108173, https://doi.org/10.1371/journal.pone.0108173, 2014.

Tang, W., Da, F., Tracey, J. C., Intrator, N., Kunes, M. A., Lee, J. A., Wan, X. S., Jayakumar, A., Friedrichs, M. A. M., and Ward, B. B.: Nutrient management offsets the effect of deoxygenation and warming on nitrous oxide emissions in a large US estuary, Sci. Adv., 10, eadq5014, https://doi.org/10.1126/sciadv.adq5014, 2024a.

Tang, W., Talbott, J., Jones, T., and Ward, B. B.: Variable contribution of wastewater treatment plant effluents to downstream nitrous oxide concentrations and emissions, Biogeosciences, 21, 3239–3250, https://doi.org/10.5194/bg-21-3239-2024, 2024b.

Teeter, L., Hamme, R. C., Ianson, D., and Bianucci, L.: Accurate Estimation of Net Community Production From O_2/Ar Measurements, Global Biogeochemical Cycles, 32, 1163–1181, https://doi.org/10.1029/2017GB005874, 2018.

Tian, H., Pan, N., Thompson, R. L., Canadell, J. G., Suntharalingam, P., Regnier, P., Davidson, E. A., Prather, M., Ciais, P., Muntean, M., Pan, S., Winiwarter, W., Zaehle, S., Zhou, F., Jackson, R. B., Bange, H. W., Berthet, S., Bian, Z., Bianchi, D., Bouwman, A. F., Buitenhuis, E. T., Dutton, G., Hu, M., Ito, A., Jain, A. K., Jeltsch-Thömmes, A., Joos, F., Kou-Giesbrecht, S., Krummel, P. B., Lan, X., Landolfi, A., Lauerwald, R., Li, Y., Lu, C., Maavara, T., Manizza, M., Millet, D. B., Mühle, J., Patra, P. K., Peters, G. P., Qin, X., Raymond, P., Resplandy, L., Rosentreter, J. A., Shi, H., Sun, Q., Tonina, D., Tubiello, F. N., van der Werf, G. R., Vuichard, N., Wang, J., Wells, K. C., Western, L. M., Wilson, C., Yang, J., Yao, Y., You, Y., and Zhu, Q.: Global nitrous oxide budget (1980–2020), Earth System Science Data, 16, 2543–2604, https://doi.org/10.5194/essd-16-2543-2024, 2024.

Uhlig, C. and Loose, B.: Using stable isotopes and gas concentrations for independent constraints on microbial methane oxidation at Arctic Ocean temperatures, Limnol. Oceanogr. Methods, 15, 737–751, https://doi.org/10.1002/lom3.10199, 2017.

NDBC: https://www.ndbc.noaa.gov/station_page.php?station=44022, last access: 4 October 2025.

Valentine, D. L.: Emerging Topics in Marine Methane Biogeochemistry, Annual Review of Marine Science, 3, 147–171, https://doi.org/10.1146/annurev-marine-120709-142734, 2011.

Vaquer-Sunyer, R. and Duarte, C. M.: Thresholds of hypoxia for marine biodiversity, Proceedings of the National Academy of Science, 105, 15452–15457, 2008.

Varekamp, J. C., McElroy, A. E., Mullaney, J. R., and Breslin, V. T.: Metals, Organic Compounds, and Nutrients in Long Island Sound: Sources, Magnitudes, Trends, and Impacts, in: Long Island Sound, edited by: Latimer, J. S., Tedesco, M. A., Swanson, R. L., Yarish, C., Stacey, P. E., and Garza, C., Springer New York, New York, NY, 203–283, https://doi.org/10.1007/978-1-4614-6126-5_5, 2014.

Vlahos, P., Whitney, M. M., Menniti, C., Mullaney, J. R., Morrison, J., and Jia, Y.: Nitrogen budgets of the Long Island Sound estuary, Estuarine, Coastal and Shelf Science, 232, 106493, https://doi.org/10.1016/j.ecss.2019.106493, 2020.

Wallace, R. B.: Coastal Ocean Acidification: Dynamics and Potential to Affect Marine Mollusks, State University of New York at Stony Brook, 2020.

Wallace, R. B. and Gobler, C. J.: The role of algal blooms and community respiration in controlling the temporal and spatial dynamics of hypoxia and acidification in eutrophic estuaries, Marine Pollution Bulletin, 172, 112908, https://doi.org/10.1016/j.marpolbul.2021.112908, 2021.

Wan, X. S., Sheng, H.-X., Dai, M., Casciotti, K. L., Church, M. J., Zou, W., Liu, L., Shen, H., Zhou, K., Ward, B. B., and Kao, S.-J.: Epipelagic nitrous oxide production offsets carbon sequestration by the biological pump, Nat. Geosci., 16, 29–36, https://doi.org/10.1038/s41561-022-01090-2, 2023a.

Wan, X. S., Sheng, H.-X., Liu, L., Shen, H., Tang, W., Zou, W., Xu, M. N., Zheng, Z., Tan, E., Chen, M., Zhang, Y., Ward, B. B., and Kao, S.-J.: Particle-associated denitrification is the primary source of N2O in oxic coastal waters, Nat Commun, 14, 8280, https://doi.org/10.1038/s41467-023-43997-3, 2023b.

Wanninkhof, R.: Relationship between wind speed and gas exchange over the ocean revisited, Limnology and Oceanography: Methods, 12, 351–362, https://doi.org/10.4319/lom.2014.12.351, 2014.

Wanninkhof, R., Asher, W. E., Ho, D. T., Sweeney, C., and McGillis, W. R.: Advances in Quantifying Air-Sea Gas Exchange and Environmental Forcing, Annual Review of Marine Science, 1, 213–244, https://doi.org/10.1146/annurev.marine.010908.163742, 2009.

Ward, B. B.: Nitrification in Marine Systems, in: Nitrogen in the Marine Environment, edited by: Capone, D. G., Bronk, D. A., Molholland, M. R., and Carpenter, E. J., Elsevier, 199–261, 2008.

Ward, B. B., Kilpatrick, K. A., Novelli, P. C., and Scranton, M. I.: Methane Oxidation and Methane Fluxes in the Ocean Surface-Layer and Deep Anoxic Waters, Nature, 327, 226–229, 1987.

Weiss, R. F. and Price, B. A.: Nitrous oxide solubility in water and seawater, Marine Chemistry, 8, 347–359, https://doi.org/10.1016/0304-4203(80)90024-9, 1980.

West, W. E., Creamer, K. P., and Jones, S. E.: Productivity and depth regulate lake contributions to atmospheric methane, Limnology and Oceanography, 61, S51–S61, https://doi.org/10.1002/lno.10247, 2016.

Whitney, M. M. and Vlahos, P.: Reducing Hypoxia in an Urban Estuary Despite Climate Warming, Environ. Sci. Technol., 55, 941–951, https://doi.org/10.1021/acs.est.0c03964, 2021.

Wiesenburg, D. A. and Guinasso, N. L.: Equilibrium solubilities of methane, carbon monoxide, and hydrogen in water and sea water, Journal of Chemical & Engineering Data, 24, 356–360, https://doi.org/10.1021/je60083a006, 1979.

de Wilde, H. P. J. and de Bie, M. J. M.: Nitrous oxide in the Schelde estuary: production by nitrification and emission to the atmosphere, Marine Chemistry, 69, 203–216, https://doi.org/10.1016/S0304-4203(99)00106-1, 2000.

Wilke, C. R. and Chang, P.: Correlation of diffusion coefficients in dilute solutions, AIChE Journal, 1, 264–270, https://doi.org/10.1002/aic.690010222, 1955.

Wilson, R. E., Swanson, R. L., and Crowley, H. A.: Perspectives on long-term variations in hypoxic conditions in western Long Island Sound, Journal of Geophysical Research: Oceans, 113, https://doi.org/10.1029/2007JC004693, 2008.

Wrage, N., Velthof, G., and Van Beusichem, M.: Role of nitrifier denitrification in the production of nitrous oxide, Soil Biology and …, 2001.

Yin, H., Wang, Y., and Huang, J.: Photodegradation-induced biological degradation of treated wastewater effluent organic matter in receiving waters, Water Research, 204, 117567, https://doi.org/10.1016/j.watres.2021.117567, 2021.

Young, C., Martin, J. B., and Hanson, G. N.: Controls on Nitrous Oxide Production in, and Fluxes from a Coastal Aquifer in Long Island, NY, USA, Journal of Marine Science and Engineering, 4, 71, https://doi.org/10.3390/jmse4040071, 2016.

Yu, C., He, Q., Nie, W.-B., Zhang, T., Wu, H., Yang, Y., Fu, S., Tan, X., and Chen, Y.: Effluent organic matter facilitates anaerobic methane oxidation coupled with nitrous oxide reduction in river sediments, Water Research, 278, 123415, https://doi.org/10.1016/j.watres.2025.123415, 2025.

Zakem, E. J. and Follows, M. J.: A theoretical basis for a nanomolar critical oxygen concentration, Limnology and Oceanography, 62, 795–805, https://doi.org/10.1002/lno.10461, 2017.

Zakem, E. J., Mahadevan, A., Lauderdale, J. M., and Follows, M. J.: Stable aerobic and anaerobic coexistence in anoxic marine zones, ISME J, 14, 288–301, https://doi.org/10.1038/s41396-019-0523-8, 2020.

Zheng, X., Mei, B., Wang, Y., Xie, B., Wang, Y., Dong, H., Xu, H., Chen, G., Cai, Z., Yue, J., Gu, J., Su, F., Zou, J., and Zhu, J.: Quantification of N2O fluxes from soil–plant systems may be biased by the applied gas chromatograph methodology, Plant Soil, 311, 211–234, https://doi.org/10.1007/s11104-008-9673-6, 2008.

Zheng, Y., Wu, S., Xiao, S., Yu, K., Fang, X., Xia, L., Wang, J., Liu, S., Freeman, C., and Zou, J.: Global methane and nitrous oxide emissions from inland waters and estuaries, Global Change Biology, 28, 4713–4725, https://doi.org/10.1111/gcb.16233, 2022.